Analysis of Relaxed User Orthogonality for Wireless Multi-user MIMO Downlink Transmission

by

Jordan Clarke

A thesis submitted to the
Department of Electrical and Computer Engineering
in conformity with the requirements for
the degree of Master of Applied Science

Queen's University
Kingston, Ontario, Canada
September 2019

Abstract

Efficient resource allocation at the physical layer of wireless communication systems is closely linked to performance. Time and space are examples of such resources. In a densely-deployed multi-antenna, multi-user wireless downlink, finding a low-interference group of spatially distributed users in conjunction with spatial-domain multiple access beamforming represent techniques for efficient use of spatial resources. However, in practice, finding a perfectly orthogonal interference-free group of users to receive concurrent service is unlikely, thus wasting the transmission period or temporal resource. In this work, we set out to analyze the allocation of competing spatial and temporal resources in the context of the wireless downlink. The intention of this analysis is to investigate the orthogonality criteria that underpin many practical user selection algorithms. Deeper understanding of such criteria has potential for designing improved interference-mitigating algorithms in this sense, and in other related scenarios. A relaxed definition of orthogonality between users in group is investigated for practical amplitude and quadrature modulation schemes. Motivated by widely-linear processing techniques, new relaxed user orthogonality on the complex hyper-sphere illustrates temporal benefits and trade-offs associated with various system parameters. Beamforming and user selection are analyzed jointly for key scenarios of interest to gain insights into the interaction between these spatial resource

management techniques. System throughput and reliability performance analysis is also developed, and applied to these scenarios to gain further insights.

Acknowledgments

First and foremost, I would like to acknowledge and thank Dr. Steven Blostein for his support throughout the course of this work. Without the experienced recommendations, patient mentorship, and generous financial support provided by Dr. Blostein, this work would not have been possible. I would also like to thank Queen's University and the Government of Ontario for supporting this work financially.

I would also like to thank my peers in the Information Processing and Communications Laboratory at Queen's, especially Matthew Quarisa, Sayed Saeed Rezazadeh, Philip Oni, Monica Rao, Mohamed Hedayati, and Tianda Li for taking time from their busy schedules to discuss and share ideas regarding this work.

The comments and feedback provided by the faculty members in Queen's Electrical and Computer Engineering Department are greatly appreciated. I would like to thank these faculty members for taking the time to review this work. I would also like to acknowledge their comments and suggestions contributing to this work.

Finally, I would like to thank my family and friends for their support over the course of this work. I would especially like to thank my parents, my Aunt Lynn and Uncle Denis, John McCrae, Ian Goode, and Ian Maquinez.

All of these sources of support has resulted in a valuable educational experience for which I am exceptionally grateful.

Contents

Abstract **i**

Acknowledgments **iii**

Contents **iv**

List of Figures **vi**

List of Acronyms and Abbreviations **ix**

Chapter 1: Introduction **1**
1.1 Motivation 1
1.2 Problem description 2
1.3 Contributions and structure 3
1.3.1 Contributions 3
1.3.2 Structure 5

Chapter 2: Background **6**
2.1 Beta functions and the Beta Distribution 6
2.2 Linear algebra 9
2.2.1 Quadratic Forms 9
2.2.2 Matrix operations and decomposition 10
2.3 Improper random variables and widely-linear processing 11
2.4 Related work on transmit beamforming and user selection 13
2.5 Notation 15

Chapter 3: System Model **18**
3.1 *Quadrature-Valued System* Model 25
3.2 *Real-Valued System* Model 26

Chapter 4: Analysis of REO and QEO Group Existence Probability **28**
4.1 Random sphere packing formulation 32

4.2 Fractional cap cover . . . 34
4.2.1 Geometric expressions for real 2-sphere and real 3-sphere . . . 34
4.2.2 Geometric approach on the real hyper-sphere . . . 36
4.2.3 New Statistical approach on the complex hyper-sphere . . . 37
4.2.4 Method based on Monte-Carlo integration . . . 41
4.2.5 Numerical and simulated results . . . 42
4.3 Dependent groups . . . 46
4.3.1 Numerical and simulated results . . . 51
4.4 Chapter summary . . . 53

Chapter 5: SDMA Beamforming **55**
5.1 MRTBF and WL-MRTBF . . . 56
5.2 RZFBF . . . 57
5.3 WL-RZFBF . . . 59
5.4 Joint analysis of beamforming and user orthogonality for maximum interference power case . . . 60
5.4.1 RZFBF analysis . . . 61
5.4.2 MRTBF analysis . . . 64
5.4.3 WL-RZFBF analysis . . . 65
5.4.4 Numerical results . . . 67

Chapter 6: System Performance Analysis **70**
6.1 Symbol Error Rate . . . 70
6.1.1 SER for maximum interference power case . . . 71
6.1.2 Numerical results for maximum interference power case . . . 73
6.2 Outage rate . . . 78
6.2.1 Numerical results for maximum interference power case . . . 79
6.3 Mean Sum Rate . . . 81
6.3.1 Numerical results for maximum interference power case . . . 81

Chapter 7: Conclusions and Future Work **86**
7.1 Conclusions . . . 86
7.2 Future Work . . . 87

Bibliography **89**

List of Figures

3.1 Block diagram of the downlink system model. 19

3.2 QPSK constellation 20

3.3 16-QAM constellation 20

3.4 BPSK constellation. 21

3.5 4-PAM constellation. 21

4.1 Definition of spherical cap $\mathcal{C}_{i_r}$ on the surface $\mathcal{S}^N$. 31

4.2 $2\frac{\Omega^N(\theta_q)}{\Omega^N(\pi)}$ and $2\frac{\Omega^N(\theta_r)}{\Omega^N(\pi)}$ given in Theorems 1 and 2 respectively, versus ϵ-orthogonality (continuous curves). 40,000-trial Monte-Carlo simulation computed according to Eq. 4.40 (discrete points). 43

4.3 Analytic RVS $p_\perp$ plotted (continuous curves) as a function of ϵ_r. 10,000-trial Monte-Carlo simulation computed according to Eq. (4.40) (discrete points). 45

4.4 $Pr[\mathscr{S}_\epsilon \neq \emptyset]$ for $L = 4$, $K = 30$ plotted as a function of ϵ. Continuous analytic curves are a lower-bound on group existence probability given by Eq. (4.54). 80,000-trial Monte-Carlo simulation computed according to Eq. (4.40) (discrete points). 52

5.1 Analytic RZFBF of signal (left) and interference (right) gains from Proposition 1 as a function of ϵ_q, $L = 4$, $N = 16$, $P_{RZF} = L$.. 68

6.1 RVS SER given by Eq. 6.1 plotted against SIR measure in terms of ϵ_r for various numbers of antennas WL-MRTBF (left) and WL-RZFBF (right). BPSK, SNR = 10dB, $L = 8$, and $\tau = \sigma^2$ are assumed. 74

6.2 QVS SER given by Eq. 6.1 (left plot) plotted against SIR measure in terms of ϵ_q. MRTBF, SNR = 10dB, and $N = 4$ are assumed. RVS SER given by Eq. 6.1 (right plot) plotted against SIR measure in terms of ϵ_r. WL-MRTBF, SNR = 10dB, and $N = 4$ are assumed. 76

6.3 QVS SER given by Eq. 6.1 (left) plotted against SIR measure in terms of ϵ_q. RZFBF, SNR = 10dB, and $N = 4$ are assumed. RVS SER given by Eq. 6.1 (right) plotted against SIR measure in terms of ϵ_r. WL-RZFBF, SNR = 10dB, $N = 4$, and $\tau = \sigma^2$ are assumed. 77

6.4 RVS and QVS single-user outage rate (bits per channel use) given by Eq. (6.8) plotted as a function of user orthogonality constraint ϵ. RZFBF assumed for QVS, WL-RZFBF assumed for RVS, $N = 16$, SNR= 10dB, and $\tau = \sigma^2$. 80

6.5 QVS mean sum rate (bits per channel use) given by Eq. (6.9) (right plot) plotted as a function of ϵ_q for MRTBF. $N = 16$, $K = 30$, SNR=10dB. RVS mean sum rate (bits per channel use) given by Eq. (6.9) (left plot) plotted as a function of ϵ_r for WL-MRTBF. $N = 16$, $K = 30$, SNR=10dB. 82

6.6 QVS mean sum rate (bits per channel use) given by Eq. (6.9) (left plot) plotted as a function of ϵ_q for RZFBF, $N = 16$, $K = 30$, SNR=10dB. RVS mean sum rate (bits per channel use) given by Eq. (6.9) (right plot) plotted as a function of ϵ_q for WL-RZFBF, $N = 16$, $K = 30$, SNR=10dB, and $\tau = \sigma^2$ 85

List of Acronyms and Abbreviations

- Multiple-input multiple-output (MIMO)
- Multi-user multiple-input multiple-output (MU-MIMO)
- Massive multi-user multiple-input multiple-output (MMU-MIMO)
- Symbol error rate (SER)
- Signal-to-noise ratio (SNR)
- Signal-to-interference ratio (SIR)
- Signal-to-interference plus noise ratio (SINR)
- Quadrature-epsilon-orthogonal (QEO)
- Real-epsilon-orthogonal (REO)
- Quadrature-valued system (QVS)
- Real-valued system (RVS)
- Widely-linear (WL)
- Beamforming (BF)
- Spatial-division multiple access (SDMA)
- Maximum-ratio transmission (MRT)
- Regularized zero-forcing (RZF)
- Quadrature phase-shift keying (QPSK)
- Binary phase-shift keying (BPSK)
- Quadrature amplitude modulation (QAM)
- Pulse amplitude modulation (PAM)

Chapter 1

Introduction

1.1 Motivation

Demand for wireless connectivity is growing with no expectation of slowing down[1]. Increasing demand for wireless connectivity is driven by several existing and emerging applications including the internet of things (IoT), vehicular networks, wireless sensor networks, automation, e-health and body-area networks, and high-throughput video applications such as streaming high-definition video and augmented reality [2]. This diverse variety of applications not only increases overall wireless demand, it also translates to a wide range of distinct quality of service (QoS) requirements in terms of power efficiency, spectral efficiency, throughput, and latency in the wireless downlink. For example, real-time applications such as autonomous vehicles require low latency communication between nodes in the network. In the case of autonomous vehicles, communication latency is an important safety factor. Sufficiently high network latency will result in out-of-date information at one or more vehicles in the network, increasing the risk of a collision. Conversely, consider streaming HD video to a wireless device. Assuming a sufficiently large buffer at the receiver, latency is

less important than high-throughput QoS.

The proliferation of interconnected wireless devices is expected to have a significant impact on the density of future wireless networks. As the number of wireless users demanding a broad range of services increases, the environment of future wireless networks is expected to be a dense deployment of co-existing networks, each designed to meet the QoS requirement of the users it is serving [3, 4, 5, 6]. Performance of such co-existing networks is expected to be interference-limited. Thus, low-level interference mitigation at the physical layer is a key challenge to overcome.

1.2 Problem description

Much work has been dedicated to physical layer interference mitigation in the wireless downlink. Such work is typically focused on taking advantage of orthogonal domains such as time (scheduling), frequency (spectral re-use), power (non-orthogonal multiple access), and space. Spatial-domain interference mitigation techniques are an active topic of investigation. One such technique is the utilization of massive multi-user multiple-input multiple-output (MMU-MIMO) and spatial-division multiple access (SDMA) to achieve a spatial multiplexing gain in the system[7, 8]. Another technique is to select users for the group based on spatial-domain orthogonality criteria. Analysis of spatial user orthogonality criteria and SDMA beamforming constitute the primary focus of this work.

Rather than developing user selection algorithms as in [9, 10, 11], the focus of this work is to investigate the spatial orthogonality criteria between a typical group of users, which is the basis for many interference-mitigating user selection algorithms. This analysis is then put in context by characterizing the interaction between spatial

user orthogonality criteria, MU-MIMO SDMA transmit beamforming, and modulation in terms of system performance on an average basis for the specific scenarios of interest. The object of this integrated approach is to gain insight into the interactions between the various facets of the larger system in terms of performance assuming a dense deployment of wireless users requesting high-throughput service and MU-MIMO. We set out to develop an analysis that scales well with the number of antennas in a system. Such an approach allows for application of the work to MMU-MIMO scenarios in the future. Spatial user orthogonality is approached as an allocation problem between competing spatial and temporal resources. The objective of a user selection algorithm is to find a group of users whose random channels are sufficiently orthogonal to mitigate interference without being so strict that we are unable to find a group of users and waste the transmission period. To analyze this problem inherent to specific user selection algorithms, a relaxed ϵ-orthogonal definition of spatial user orthogonality is adopted, similar to [12], with several improvements, extensions, and further contributions.

1.3 Contributions and structure

1.3.1 Contributions

The contributions of this work are as follows:

1. System performance is analyzed using an integrated approach, investigating the interaction between modulation, beamforming, and user orthogonality. Performance analysis features symbol error rate (SER), single user capacity, and mean group sum rate characterization. A variety of practical discrete-alphabet real

and quadrature modulation schemes are considered. The analysis also characterizes several linear beamforming schemes and two definitions of spatial user orthogonality criteria.

2. For the first time, an exact expression for widely-linear fractional cap cover on the N-dimensional complex hypersphere is developed by extending works [13, 14, 15] and applying widely-linear processing techniques [16, 17, 18]. Numerical computation of this expression scales well with the number of antennas in the system, which is attractive in the context of the MMU-MIMO system. This new result is applied to user orthogonality analysis to illustrate performance benefits associated with judiciously designing user orthogonality criteria in conjunction with modulation and beamforming schemes utilized in the system.

3. The union bound in [12] is substituted for a criterion that loosens strict orthogonality to a mean-based metric. By making use of this mean-based approach, we avoid several problems associated with orthogonality definition in terms of non-overlapping randomly placed spherical caps. The location of caps on the sphere are randomly placed when forming a group of users based on relaxed orthogonality criteria. This is not the case in the well-known sphere packing problem in the context of channel coding [19] or more recently in [20]. The location of codewords is chosen, thus allowing for a non-overlapping packing to be found without gaps between codewords in the spherical space. We do not have such control when forming relaxed orthogonality groups of users, thus finding a strictly non-overlapping packing is a difficult task. Instead, a certain degree of overlap between caps is allowed on an average basis, making the problem much more tractable. This approach also avoids the issue of neglecting intersections

of more than two caps for groups of more than two users.

1.3.2 Structure

The remainder of the work is organized into six chapters. First, background information and related work are reviewed. Next, system models and preliminary assumptions are presented. The system structure, channel model, user selection, and modulation schemes are formulated in the context of these models. User orthogonality is then formulated as a random packing problem assuming hyper-spherical model and analyzed. Following relaxed user orthogonality analysis, several beamforming models are developed and analyzed. Beamforming and user orthogonality analyses are then used to characterize overall system performance. Lastly, conclusions and future work are discussed.

Chapter 2

Background

The first several sections of this chapter are concerned with the provision and explanation of reference material used throughout the work. These sections provide a more detailed supporting explanation of methods and concepts applied in later chapters. The final section of this chapter conducts a brief survey of existing work in the field that is related to this work.

2.1 Beta functions and the Beta Distribution

The Beta Distribution and various Beta functions are useful in a variety of applications, including stochastic quadratic forms. It is important to differentiate between the Beta Distribution, the Beta Function, the Incomplete Beta Function, and the Incomplete Regularized Beta Function. The Beta Distribution is a continuous probability distribution that is defined on the interval $[0, 1]$ [15]. The probability density function (PDF) and cumulative distribution function (CDF) of the Beta Distribution are given in terms of the various Beta functions.

For a random variable, X that is Beta- distributed with shape parameters a and b, we adopt the notation $X \sim \beta(a, b)$. Let $x \in X$ be the realizations of X and denote

$f_X(x)$ as the PDF of X. We also define $F_X(x)$ as the CDF of X.

The PDF and CDF of $X \sim \beta(a, b)$ is described in terms of the Beta Function, and Incomplete Regularized Beta Function. We define $B(a, b)$ as the Beta Function, $B_x(a, b)$ as the Incomplete Beta Function, $I_x(a, b)$ as the Incomplete Regularized Beta Function, and $\Gamma(z)$ as the Gamma Function. $B(a, b)$ can be described in several ways. For example, $B(a, b)$ can be described in terms of the Gamma function as

$$B(a, b) \equiv \frac{\Gamma(a)\Gamma(b)}{\Gamma(a + b)}, \tag{2.1}$$

where

$$\Gamma(z) \equiv \int_0^\infty y^{z-1} e^{-y} dy \quad \forall \ \mathrm{Re}\{z\} > 0. \tag{2.2}$$

Alternatively, the Beta Function can be represented in the trigonometric form

$$\begin{aligned} \mathrm{B}(a, b) = 2 \int_0^{\frac{\pi}{2}} \sin^{2b-1}(\phi) \cos^{2a-1}(\phi) \ d\phi \\ \forall \ a > 0, \ b > 0 \ . \end{aligned} \tag{2.3}$$

The trigonometric form of $B(a, b)$ leads to the Incomplete Beta Function

$$\begin{aligned} \mathrm{B}_x(a, b) = 2 \int_0^{x} \sin^{2b-1}(\phi) \cos^{2a-1}(\phi) \ d\phi \\ \forall \ a > 0, \ b > 0, \end{aligned} \tag{2.4}$$

where $B_{\frac{\pi}{2}}(a, b) = B(a, b)$. The Incomplete Regularized Beta function is

$$\mathrm{I}_x(a, b) \equiv \frac{\mathrm{B}_x(a, b)}{\mathrm{B}_{\frac{\pi}{2}}(a, b)} \quad . \tag{2.5}$$

Given $X \sim \beta(a, b)$ the PDF and CDF of X are

$$f_X(x) \equiv \frac{x^{a-1}(1-x)^{b-1}}{B(a,b)}, \tag{2.6}$$

$$F_X(x) = \mathrm{I}_x(a, b), \tag{2.7}$$

respectively [15]. The mean and variance of $X \sim \beta(a, b)$ are

$$\mathrm{E}\{X\} = \frac{a}{a+b}, \tag{2.8}$$

and

$$\mathrm{E}\{X^2\} = \frac{ab}{(a+b)^2(a+b+1)}, \tag{2.9}$$

respectively [15], where $\mathrm{E}\{\cdot\}$ is the statistical expectation.

When $a \neq b$, the Beta Distribution is said to be skewed. When $X \sim \beta(a, b)$ and $a < b$, the distribution is said to have a positive skew. Most of the mass in the PDF is skewed towards zero, that is, $\mathrm{E}\{X\} < 0.5$ and $f_X(x)$ is a monotonically decreasing function of x that has a shape similar to a mirrored letter 'J'.

The mirroring property [15] is an important property of the Beta Distribution in the context of this work.

Definition 1. *Mirroring Property of the Beta distribution*
Given Beta-distributed random variable, $X \sim \beta(a, b)$, then

$$1 - X \sim \beta(b, a) \tag{2.10}$$

2.2 Linear algebra

2.2.1 Quadratic Forms

In the context of this work, the term "quadratic forms" refers to inner products and norms of vectors. Given two vectors $\underline{x}$ and $\underline{y}$, the inner product between $\underline{x}$ and $\underline{y}$ is defined as $< \underline{x}, \underline{y} >$. Assuming $\underline{x}, \underline{y} \in \mathbb{C}^n$, where $\mathbb{C}^n$ is the n-dimensional complex Hilbert Space, their inner product is

$$< \underline{x}, \underline{y} >= \underline{x}^H \underline{y} \tag{2.11}$$

where, $\underline{x}^H$ is the conjugate transpose (Hermitian) of $\underline{x}$. In general, the product in Eq. (2.11) is a complex scalar value. The magnitude of this product, which is a real scalar quantity, is calculated

$$\|\underline{x}^H \underline{y}\| = \sqrt{(\underline{x}^H \underline{y})(\underline{x}^H \underline{y})^*}, \tag{2.12}$$

where $(\underline{x}^H \underline{y})^*$ is the conjugate of $(\underline{x}^H \underline{y})$.

The L-2 norm of $\underline{x}$, which is a real scalar quantity, is given by

$$\|\underline{x}\| = \sqrt{\underline{x}^H \underline{x}}. \tag{2.13}$$

Asserting the Cauchy-Schwarz inequality, the normalized inner product is given by

$$\frac{\|\underline{x}^H \underline{y}\|}{\|\underline{x}\| \|\underline{y}\|} \in [0, 1]. \tag{2.14}$$

2.2.2 Matrix operations and decomposition

Given the $n \times l$ matrix, $\mathbf{X}$, we define the trace of the matrix as

$$\mathrm{Tr}(\mathbf{X}) \equiv \begin{cases} \sum_{i=1}^{n} \mathbf{X}_{i,i}, & \text{if } n > l \\ \sum_{i=1}^{l} \mathbf{X}_{i,i}, & \text{otherwise} \end{cases} \tag{2.15}$$

where $(\mathbf{X})_{i,i}$ denotes the i^{th} diagonal element of the matrix $\mathbf{X}$. The rank of $\mathbf{X}$ is given by $\mathrm{Ra}(\mathbf{X})$.

We define $\mathbf{X}^{\dagger}$and $\mathbf{X}^{\ddagger}$ as the Moore-Penrose left pseudo-inverse and Moore-Penrose right pseudo-inverse of $\mathbf{X}$, respectively, given by

$$\mathbf{X}^{\dagger} = (\mathbf{X}^{H}\mathbf{X})^{-1}\mathbf{X}^{H}, \tag{2.16}$$

and

$$\mathbf{X}^{\ddagger} = \mathbf{X}^{H}(\mathbf{X}\mathbf{X}^{H})^{-1}. \tag{2.17}$$

When $l > n$, we have $\mathbf{X}^{\dagger}\mathbf{X} = \mathbf{I}$, and conversely when $n > l$ we have $\mathbf{X}\mathbf{X}^{\ddagger} = \mathbf{I}$, where $\mathbf{I}$ is the identity matrix. When $l = n$ $\mathbf{X}$ is square and assuming $\mathbf{X}$ is invertible we have $\mathbf{X}^{\dagger} = \mathbf{X}^{\ddagger} = \mathbf{X}^{-1}$.

Assume that the $l = n$ (i.e. $\mathbf{X}$ is square), $\mathrm{Ra}(\mathbf{X}) = n$ (i.e. $\mathbf{X}$ is full rank), $\mathbf{X}$ is hermitian and $\mathbf{X}$ is invertible. In this case, $\mathbf{X}$ will have n eigenvalues, corresponding to n linearly-independent $n \times 1$ eigenvectors. We define λ_i as the i^{th} scalar eigenvalue of $\mathbf{X}$ belonging to the i^{th} eigenvector defined as $\underline{e}_i$. The eigen decomposition of $\mathbf{X}$ is given by

$$\mathbf{X} = \sum_{i=1}^{n} \lambda_i \underline{e}_i \underline{e}_i^{H}. \tag{2.18}$$

The inverse of $\mathbf{X}$ and also be written as

$$\mathbf{X}^{-1} = \sum_{i=1}^{n} \frac{1}{\lambda_i} \underline{e}_i \underline{e}_i^H . \tag{2.19}$$

2.3 Improper random variables and widely-linear processing

Complex random variables can be classified as circularly-symmetric, proper, or improper. A proper random variable is uncorrelated with its complex conjugate, and its real and imaginary parts have the same finite variance (i.e., the complex random variable has a constant diagonal covariance matrix). Conversely an improper complex random variable has a covariance matrix that does not satisfy these criteria [21]. Circular-symmetric complex variables are proper by definition; however, the criteria for circularly symmetry is more strict. For a complex random variable to be circularly-symmetric, its PDF must be rotation-invariant about the origin in the complex plane.

In the context of communications, random variable properties are of particular interest when processing complex signals. A common example is decoding symbols at a receiver that are corrupted with random noise. In practice, symbols may be chosen from a real or quadrature alphabet. The statistics used to process signals, depend on whether a quadrature or real modulation scheme is chosen [22, 23]. Thus, processing quadrature-modulated signals modelled as statistically proper is sufficient; however, when processing amplitude-modulated signals, we must consider improper random variables.

Whether or not a complex random variable is proper is important in the context of linear minimum mean-square estimation (LMSE). Suppose we are given a scalar

random estimand Y that is a linear combination of random observations $\underline{X}$ such that

$$Y = \underline{h}^H \underline{X}. \tag{2.20}$$

The object of the LMSE problem is to generate an estimate for Y, $\hat{Y}_L$, that minimizes $\mathrm{E}\{(Y - \hat{Y}_L)^2\}$. We assume that the elements of $\underline{X}$ are complex random variables with realizations $\underline{x}$. Thus, the LMSE problem can be written as

$$\hat{Y}_L = \underline{u}^H \underline{X}, \tag{2.21}$$

where we must find $\underline{u}$ such that $\mathrm{E}\{(Y - \hat{Y}_L)^2\}$ is minimized. By the orthogonality principle, this solution will be achieved when $\mathrm{E}\{(Y - \hat{Y}_L)^2\} \perp \underline{X}$. Arriving at such a solution is a well-known problem that can be solved by recursive regression on $\mathrm{E}\{Y|\underline{X}\}$ [24]. However, when the elements of $\underline{X}$ are realized from an improper random variable, the linear structure in Eq. (2.20) is no longer able to achieve a minimum mean-squared error solution [17]. Since $\underline{X}$ has non-zero correlation with $\underline{X}^*$, we must take advantage of this correlation to arrive at the minimum-mean squared error solution. In order to do so, we formulate a wide-sense linear (or widely-linear) minimum mean-squared estimation problem (WLMSE). In WLMSE, we have

$$Y = \underline{h}^H \underline{X} + \underline{g}^H \underline{X}^*. \tag{2.22}$$

Similar to Eq. (2.21), we write the WLMSE problem as

$$\hat{Y}_{WL} = \underline{u}^H \underline{X} + \underline{v}^H \underline{X}^*, \tag{2.23}$$

where we must find $\underline{u}$ and $\underline{v}$ such that $\mathrm{E}\{(Y - \hat{Y}_{WL})^2\}$ is minimized. The solution to the WLMSE problem has been investigated at length in several works including [17].The case where Y is real, assuming the elements of $\underline{X}$ are improper realizations is of particular interest. In this case, $\underline{u} = \underline{v}^*$ [17], thus Eq. (2.23) becomes

$$\hat{Y}_{WL} = 2\mathrm{Re}\{\underline{u}^H \underline{X}\}. \tag{2.24}$$

In the context of digital wireless communications systems, the result in Eq. (2.24) is particularly interesting for designing multiple-input multiple-output (MIMO) linear pre-coding schemes for amplitude modulation. Given a complex realization of the wireless channel, a complex pre-coding vector can be designed to estimate the real amplitude modulated estimand in Eq. (2.24). The same principle can also be applied to user selection schemes designed to mitigate interference. When demodulating the amplitude-modulated signal, only the real part of interference impacts demodulation performance. Therefore, when users transmitting amplitude-modulated signals are selected in terms of complex channel realizations, widely linear techniques can be applied to mitigate interference in a fashion better suited to the amplitude-modulated signal.

2.4 Related work on transmit beamforming and user selection

Optimal transmit beamforming is a well-known problem, it is the subject of many works including [25]. Several conventional linear transmit beamforming schemes include maximum-ratio transmit beamforming (MRTBF), zero-forcing beamforming (ZFBF), and minimum mean-squared error beamforming (MMSEBF). Each of these

schemes is optimal in a specific sense. Unsurprisingly, there are advantages and drawbacks to each scheme. MRTBF is optimal in the signal-to-noise ratio (SNR) sense; it neglects interference. Computational complexity of MRTBF is low relative to ZFBF and MMSEBF. Conversely, ZFBF is optimal in the signal-to-interference ratio (SIR) sense; it neglects noise. In addition to incurring higher computational complexity relative to MRTBF, ZFBF also consumes an unbounded amount of transmit power when users are spatially co-located. MMSEBF is optimal in the signal-to-interference plus noise (SINR) sense, achieving minimum sum of mean-squared errors at the receiver. MMSEBF can be viewed as a weighted superposition of MRTBF and ZFBF. Although MMSEBF is well-suited to adapting to noise-limited or interference-limited environments, it requires an estimate of the noise power of the wireless channel. Estimating such a quantity accurately with low complexity is a challenging problem [26].

In general, linear transmit beamforming schemes assume the estimand observes proper statistics. This assumption holds for quadrature-modulated signals. However, when an amplitude-modulated signal is assumed, the estimand will follow an improper distribution [18]. In order to achieve MSE performance for an improper estimand, widely linear processing techniques must be employed [17, 16, 27]. Widely linear processing has been in the context of of amplitude-modulated transmit beamforming to achieve spectral efficiency competitive with quadrature modulation schemes, particularly suitable for a large group of low-throughput low-latency users [28, 29, 30, 31].

Judiciously selecting spatially-distributed users has also been shown to improve system performance in conjunction with beamforming [32, 12, 33]. In downlink user selection, a group of users is chosen by the transmitter from the large number of

densely populated candidates to receive concurrent service from the transmitter. By filtering users in terms of interference in conjunction with beamforming, the transmit beamformer is able to achieve better average spatial multiplexing gain under finite power constraints [34, 35].

There is a significant collection of works discussing the user selection problem from a variety of approaches. For example, a relaxed-orthogonality approach is taken in [12, 32, 36, 37, 33]. In [12] zero-forcing beamforming throughput performance is shown to approach that of dirty paper coding asymptotically. A similar asymptotic analysis is performed in [32] and compared to a semi-orthogonal user selection (SUS) greedy algorithm. More recent works [36, 37, 33] focus on throughput performance, making use of spherical cap packing analyses. In [36], performance of selection algorithms is studied under the assumption of imperfect channel state information (CSIT) and finite signalling alphabet (QPSK, 16-QAM). Similarly, emphasis is placed on modelling and computing SINR distributions under imperfect CSIT in [37]; however, sum rates are computed on continuous signalling alphabets. In [33], asymptotic throughput is considered (in the sense that an arbitrarily large number of candidate users are available). Again, emphasis is placed on imperfect CSIT, and continuous Gaussian signalling alphabets are implicitly assumed. Results in [33] suggest mean sum rate to be a concave function of user selection orthogonality criteria, which agrees with the hypothesis asserted in this work.

2.5 Notation

Inline description of variables and operations is given throughout the work. However, consistent notation conventions are observed as much as possible throughout the work.

A description of these conventions is provided here for further context.The following naming conventions have been adopted throughout the work:

- Upper case letters X are used to denote random variables or scalar system parameters, depending on context.
- Lower case letters $x \in X$ are used to denote realizations of random variables.
- Underline notation $\underline{x}$ is used to denote vectors.
- Bold upper case boldface letters $\mathbf{X}$ is used to denote matrices.
- $\mathbb{R}^N$ is used to denote the real N-dimensional space.
- $\mathbb{C}^N$ is used to denote the complex N-dimensional space.
- ABC font is used to denote a set.
- $\mathcal{ABC}$ font is used to denote a surface and or point in a given space.
- $\mathscr{ABC}$ font is used to denote an ensemble of sets.
- $\mathfrak{ABC}$ font is used to denote a transform in some sense.

A notable exception to the conventions are the channel variables $\underline{h}_i$, $\underline{h}_j$ used extensively throughout the following chapters. These variables are used to represent vectors of random variables. Assuming the conventions above, these variables ought to user upper case letters. The choice to use lower case letters is made to avoid confusion with upper case matrix variables representing the channel.

The following function notation conventions have also been adopted:

- $\mathrm{E}\{\cdot\}$ is used to denote the statistical expectation operation.

- $\|\cdot\|^2$ is used to denote the L-2 norm of a vector.
- $\mathrm{Re}\{\cdot\}$ is used to denote the real part of a complex value.
- $\mathrm{Im}\{\cdot\}$ is used to denote the imaginary part of a complex number.
- $|\cdot|$ is used to denote the magnitude of a complex number, the absolute value of a real number, or the carnality of a set.
- $\mathrm{Tr}(\cdot)$ is used to denote the trace of a matrix.
- $\mathrm{Ra}(\cdot)$ is used to denote the rank of a matrix.

Chapter 3

System Model

The system model assumed is illustrated in Fig. 3.1. The topology is chosen to emulate a plausible scenario in a future terrestrial wireless downlink. A large number of densely-deployed, low complexity single-antenna users require low latency, high throughput service from a massive MIMO base station transmitter with N antennas.

A spatial-division multiple-access (SDMA) scheme is assumed at the physical layer to provide concurrent service to a group of users, A, such that $|\mathsf{A}| = L$, from a larger set of candidate users, C, such that $|\mathsf{C}| = K \geq L$.

For a given transmission period, the i^{th} user in A receives symbol s_i, which is a realization of the random variable S_i. Each user receives its own stream of symbols independent of other users in A. Symbol transmit energy is assumed to be normalized with energy $E_s = E\{S_i^2\} = 1$. Symbol realizations take discrete values from a finite alphabet of size M with uniform probability. In the case of quadrature modulation we have $s_i \in \mathsf{S}_{M_q} = \{\mathsf{s}_{(1,1)}, \ldots \mathsf{s}_{(\sqrt{M},\sqrt{M})}\}$, where S_{M_q} is the quadrature signalling alphabet and $\mathsf{s}_{(1,1)}$ is the symbol at real and imaginary index 1. Similarly for amplitude modulation we have $s_i \in \mathsf{S}_{M_r} = \{\mathsf{s}_{(1)}, \ldots \mathsf{s}_{(M)}\}$, where S_{M_r} is the amplitude signalling

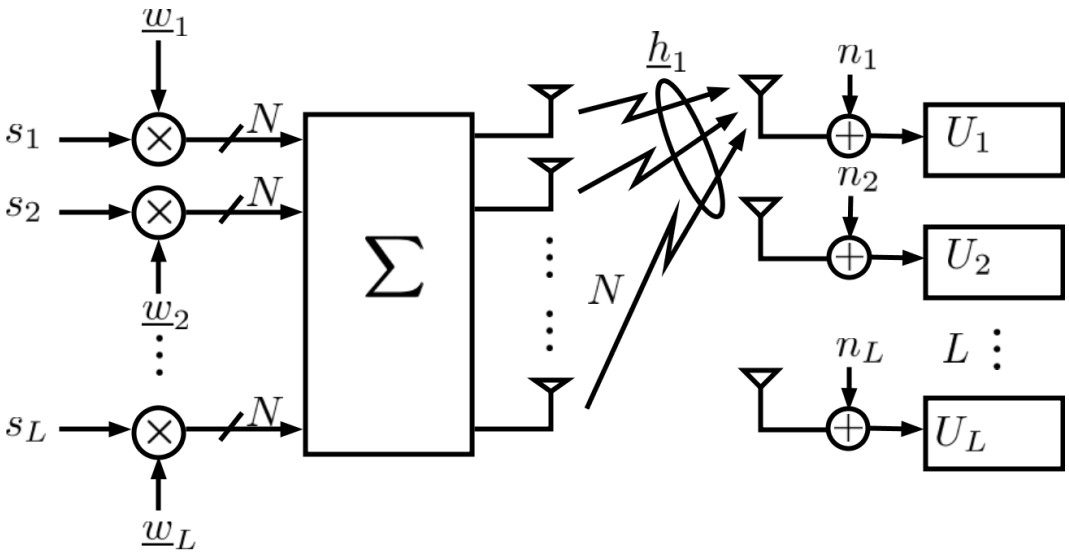

Figure 3.1: Block diagram of the downlink system model.

alphabet and $\mathsf{s}_{(1)}$ is the symbol at index 1. Gray coding is assumed. Four modulation schemes are considered without loss of generality: binary phase shift keying (BPSK), 4-symbol pulse amplitude modulation (4-PAM), quadrature phase shift keying (QPSK) and 16-symbol quadrature amplitude modulation (16-QAM). The QPSK and 16-QAM constellation diagrams are shown in Figs. 3.2 and 3.3, respectively.

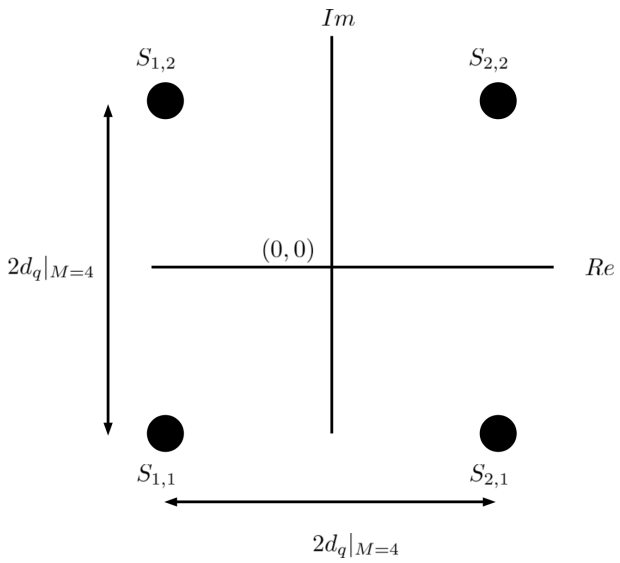

Figure 3.2: QPSK constellation

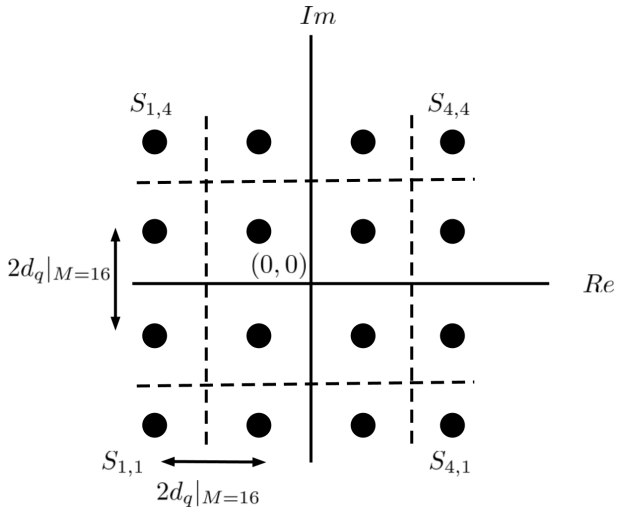

Figure 3.3: 16-QAM constellation

The constellation diagrams for the BPSK and 4-PAM schemes are shown in Fig 3.4 and Fig. 3.5, respectively.

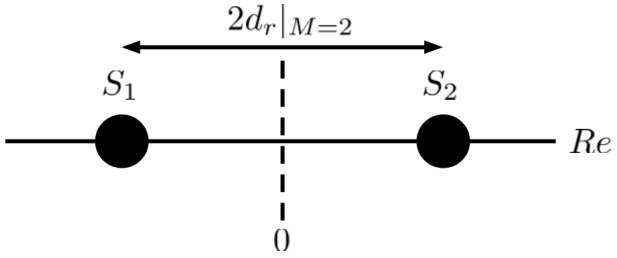

Figure 3.4: BPSK constellation.

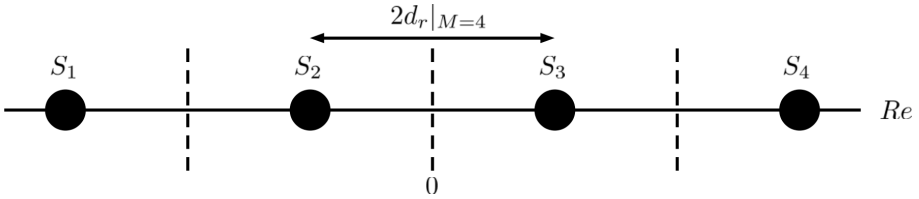

Figure 3.5: 4-PAM constellation.

Since we have assumed a uniform probability of symbol transmission across the alphabet, the decision boundaries of the Voronoi regions are equidistant between neighbouring symbols. The distance between neighbouring symbols is given by $2d_q$ for quadrature modulation and $2d_r$ for real modulation. For quadrature modulation, we assume a unit-energy baseband signalling pulse $g(t)$ is scaled by real and imaginary amplitude components, A_{m_1} and A_{m_2}, such that

$$\begin{aligned} \mathsf{s}_{(m_1,m_2)} &= (A_{m_1} + jA_{m_2})g(t) \in \mathsf{S}_{M_q} \\ &\forall\ m_1\ , m_2 = 1,\ 2 \ldots \sqrt{M}. \end{aligned} \tag{3.1}$$

We can re-write the above amplitude components as

$$\begin{aligned} A_{m_1} &= (2m_1 - 1 - \sqrt{M})d_q, \\ A_{m_2} &= (2m_2 - 1 - \sqrt{M})d_q. \end{aligned} \tag{3.2}$$

The average symbol energy is given by

$$\begin{aligned} E_s &= \frac{1}{M}\sum_{m_1=1}^{\sqrt{M}}\sum_{m_2=1}^{\sqrt{M}} A_{m_1}^2 + A_{m_2}^2 \\ &= \frac{d_q^2}{M}\sum_{m_1=1}^{\sqrt{M}}\sum_{m_2=1}^{\sqrt{M}} (2m_1 - 1 - \sqrt{M})^2 + (2m_2 - 1 - \sqrt{M})^2 \end{aligned} \tag{3.3}$$

which yields

$$\begin{aligned} d_q &= \sqrt{\frac{3E_s}{2(M-1)}} \\ &= \sqrt{\frac{3}{2(M-1)}}. \end{aligned} \tag{3.4}$$

For quadrature modulation, we assume a unit-energy baseband signalling pulse $g(t)$ is scaled by real amplitude components A_m such that

$$\mathsf{s}_{(m)} = A_m g(t) \in \mathsf{S}_{M_r}. \tag{3.5}$$

We can re-write the amplitude components as

$$\begin{aligned} A_m &= (2m - 1 - M)d_r \\ &\forall\ m = 1,\ 2 \ldots M. \end{aligned} \tag{3.6}$$

The average symbol energy is given by

$$\begin{aligned} E_s &= \frac{1}{M}\sum_{m=1}^{M} A_m^2 \\ &= \frac{d_r^2}{M}\sum_{m=1}^{M} (2m - 1 - \sqrt{M})^2, \end{aligned} \tag{3.7}$$

which yields

$$\begin{aligned} d_r &= \sqrt{\frac{3E_s}{M^2-1}} \\ &= \sqrt{\frac{3}{M^2-1}}. \end{aligned} \tag{3.8}$$

The separation between symbols in the constellations described by d_r or d_q has significant impact on the reliability performance of symbol transmission. When the separation between symbols in the constellation is low, the probability of incorrectly decoding a transmitted symbol corrupted by interference and noise increases. Thus, holding $E_s = 1$, we expect higher-order constellations to have higher symbol error rates (i.e. sacrificing power efficiency for spectral efficiency). Similarly, given $E_s = 1$ and a given constellation order, we expect the symbol error rate of a real signalling scheme to be higher than that of a quadrature signalling scheme assuming the same number of symbols in both modulation schemes.

For practical systems implementing user selection algorithms, we assume a quasi-static channel is periodically estimated, providing perfect CSIT. Motivated by this model, we assume each element in the $N \times 1$ wireless channel vector $\underline{h}_i,\ i = 1, 2 \ldots L$ is an independent identically distributed random variable following complex circularly symmetric normal distribution $\mathcal{N}_{\mathbb{C}}(0, 1)$ in order to develop an average-basis analysis. Given that each element in $\underline{h}_i$ is distributed according to circular-symmetric complex normal distribution, $\underline{h}_i$ is spherically-distributed as given by Theorem 1.5.1 [14]. The focus of this work is to study spatial-domain orthogonality and interference on an average basis, whereas others have considered power-domain orthogonality [38, 34]. We assume users have the same path loss, which is a worst-case assumption in the power-domain sense. We assume estimated vectors $\underline{h}_i$ are normalized to unity (i.e. $\|\underline{h}_i\|^2 = 1$). We do not expect groups containing dissimilar channel norms to perform

worse than those with similar ones in a spatial orthogonality sense. Therefore, we analyze user selection and transmit beamforming using normalized channel estimate vectors, neglecting the discrepancies between norms in the group. In addition to the channel vector $\underline{h}_i$, we define $\mathbf{H}$ as the $N \times L$ channel matrix whose i^{th} column is $\underline{h}_i$. Additive white Gaussian noise (AWGN) is assumed. The AWGN terms N_i, $1 \leq i \leq L$ in Fig. 3.1 are assumed to follow a complex circularly symmetric normal distribution $\mathcal{N}_{\mathbb{C}}(0, \sigma_n^2)$. Each of the L users' symbols is linearly pre-coded by a $1 \times N$ beamforming row vector, defined as $\underline{w}_i$. We also define $\mathbf{W}$ as the $L \times N$ beamforming whose i^{th} row is $\underline{w}_i$. Each of the L $N \times 1$ vectors are summed together and transmitted over $\underline{h}_i$, $i = 1, 2 \ldots L$ to the corresponding user. The received signal for the i^{th} user is given as a sum of signal, interference and noise terms

$$R_i = \underline{w}_i \underline{h}_i S_i \; + \; \sum_{j \neq i}^{L} \underline{w}_i \underline{h}_j S_j \; + \; N_i \; . \tag{3.9}$$

Since users are densely-deployed, we expect the system to be interference limited. Finding a group of users that are spatially orthogonal to some extent in conjunction with beamforming is expected to mitigate intra-group interference under finite transmit power constraints and increase system throughput. However, on average, it is highly unlikely that we will be able to find a group of perfectly orthogonal users for a given channel estimation period. This wastes transmission opportunities since the transmitter is unable to find a group suitable for interference-free transmission. Conversely, if no spatial orthogonality criterion is imposed when the group is formed, the transmitter will always be able to find a group; however, interference is likely to hinder throughput. Therefore, we propose to investigate and analyze these competing resources at the transmitter inherent to many practical user selection algorithms.

3.1 *Quadrature-Valued System* Model

We propose analysis of user selection, beamforming and modulation at the transmitter based on either quadrature or amplitude, i.e., we consider a *quadrature-valued system* (QVS) or a *real-valued system* (RVS) model. The QVS model analyzes four specific modulation schemes: binary phase shift keying (BPSK), 4-symbol pulse amplitude modulation (4-PAM), quadrature phase shift keying (QPSK) and 16-symbol quadrature amplitude modulation (16-QAM). We propose a ϵ-orthogonal criterion for forming and characterizing a group of users. The criterion is designed to mitigate intra-group interference according to Definition 2.

Definition 2. *Quadrature ϵ-orthogonal (QEO) groups of users:*
Given a pool of candidate users C*, their corresponding channel estimates* $\underline{h}_i$*, and a perspective group of users to receive concurrent service from the transmitter* A*, let us define the set of all QEO groups as*

$$\begin{aligned} \mathscr{S}_{\epsilon_q} \equiv \{\mathsf{A} \;\big|\; E\{\|\underline{h}_i^H \underline{h}_j\|^2\} \;\leq\; \epsilon_q\}, \\ \forall\; i \neq j \in \mathsf{A},\; \forall \mathsf{A} \subset \mathsf{C}, \end{aligned} \tag{3.10}$$

where $E\{\cdot\}$ denotes the expectation taken over all possible realizations of the random channel estimate.

The transmitter chooses the value of $\epsilon_q \in [0, 1]$ in Eq. (3.10) to control the allocation of resources. A choice of $\epsilon_q = 1$ places all allocation emphasis on temporal resources. Since no constraints are imposed on channel orthogonality for $\epsilon_q = 1$, we are guaranteed to always find a group of users for a given transmission period. Conversely, choosing $\epsilon_q = 0$ places all emphasis on spatial resources. When $\epsilon_q = 0$

we only allow a group with perfectly orthogonal users to be formed. In practice, this will be an extremely unlikely event, thus the probability of wasting the transmission period is very high.

Two linear transmit beamforming schemes are characterized in the QVS model: maximal-ratio transmit beamforming, and regularized zero-forcing beamforming. Beamforming analysis conditioned on the existence of a QEO group is discussed at length in Chapter 5.

3.2 *Real-Valued System* Model

The RVS model considers two specific modulation schemes: binary phase shift keying (BPSK), 4-symbol pulse amplitude modulation (4-PAM). We define an ϵ-orthogonal criterion for forming groups of users analogous to Definition 2; where, the criterion is modified to reflect the choice of a purely real modulation scheme, motivated by widely-linear processing techniques.

Definition 3. *RVS ϵ-orthogonal (REO) groups of users:*
Given a pool of candidate users C*, their corresponding channel estimates* $\underline{h}_i$*, and a perspective group of users to receive concurrent service from the transmitter* A*, let us define the set of all REO groups as*

$$\mathscr{S}_{\epsilon_r} \equiv \{\mathsf{A} \;\big|\; E\{Re\{\underline{h}_i^H \underline{h}_j\}^2\} \;\leq\; \epsilon_r\}, \quad \forall\; i \neq j \in \mathsf{A},\; \forall \mathsf{A} \subset \mathsf{C}. \tag{3.11}$$

We also define the term *ϵ-orthogonal* to describe a group of users, A, who satisfy QEO or REO user selection criteria.

Two linear transmit beamforming schemes are considered in the RVS model:

widely-linear maximum-ratio transmit beamforming and widely-linear regularized zero-forcing beamforming. Beamforming analysis conditioned on the existence of a REO group is discussed at length in Chapter 5.

Chapter 4

Analysis of REO and QEO Group Existence Probability

A statistical approach is taken towards analyzing the probability of finding REO and QEO groups as defined in Definitions 2 and 3. In order to analyze the probability that an ϵ-orthogonal group exists, several abstractions and methods are employed. User orthogonality is abstracted onto a spherical (or hyper-spherical) surface. The hyper-spherical surface of an arbitrary number of dimensions is defined in a real space for some portions of the analysis, and in other portions a complex space. Statistical analysis of orthogonality is then formulated as a random cap packing problem on the spherical surface. Instead of bounding the random packing problem as in [12], orthogonality on the surface is analyzed on an average basis. Thus, we can tractably compute the probability of finding REO and QEO groups by calculating the mean fraction of non-overlapping caps using [39]. The mean fraction of overlapping cap result in [39] depends on the fraction of the hyper-spherical surface that the cap covers. We extend methods for computing this fractional area from [13] and [14] for use in the context of this analysis. The problem at hand requires us to find an L-sized

ϵ-orthogonal group considering $\binom{K}{L}$ possible choices made from a candidate pool of size K. As noted in [12], these $\binom{K}{L}$ groups will have users in common. Therefore, statistical dependence among groups must be accounted for when calculating the probability of finding an ϵ-orthogonal group. A graph-based dependency analysis is employed using the results from [40]. The analysis culminates in the probability of finding QEO and REO groups of size L chosen from a candidate pool of K users.

Much of the spherical analysis is common between the inner products in Definitions 2 and 3. Therefore, we will introduce terms that apply to both Definition 2 and 3 rather than redundantly repeating arguments common to both definitions. First, let us define the generic user orthogonality parameters

$$\epsilon \in \{\epsilon_q, \epsilon_r\}, \tag{4.1}$$

and

$$\theta \in \{\theta_q, \theta_r\}. \tag{4.2}$$

Since the channel estimates are random, the inner product of these vectors is also random. We define the random variable $V_q = \|\underline{h}_i^H \underline{h}_j\|^2$ whose realizations are v_q. Similarly, we define the random variable $V_r = \mathrm{Re}\{\underline{h}_i^H \underline{h}_j\}^2$ whose realizations are v_r. We also define the generic inner product random variable

$$V \in \{V_q, V_r\}, \tag{4.3}$$

whose realizations are given by v. Thus the distribution of V depends on whether a

REO or QEO inner product is assumed. We also define the generic spherical cap

$$\mathcal{C}_i \in \{\mathcal{C}_{i_q},\ \mathcal{C}_{i_r}\}; \tag{4.4}$$

a more formal definition is provided in the ensuing discussion, specifically Eqs. (4.6) and (4.7) and Fig 4.1.

Given a $N \times 1$ complex vector $\underline{h}_i \in \mathbb{C}^N$, let us define the surface of the complex unit hyper-sphere in N dimensions as

$$\mathcal{S}^N \equiv \{\underline{h}_i \in \mathbb{C}^N \ : \ \|\underline{h}_i\|^2 = 1\} \ . \tag{4.5}$$

Orthogonality between pairs of vectors can be interpreted geometrically on the surface $\mathcal{S}^N$ in terms of spherical caps. A spherical cap is defined on $\mathcal{S}^N$ by first defining the point $\mathcal{P}_i \in \mathcal{S}^N$ corresponding to $\underline{h}_i$. Then a cone, with apex at the origin of the sphere, $\mathcal{O}$, and co-latitude angle θ centered along the axis of $\underline{h}_i$ is intersected with the spherical surface. This intersection defines spherical cap, $\mathcal{C}_i$. A graphical interpretation is shown in Fig. 4.1.

We define $\theta_q = \arccos(\sqrt{\epsilon}_q) \in [0, \frac{\pi}{2}]$ as the co-latitude of QEO cap, $\mathcal{C}_{i_q}$. Similarly, given the definition of $\mathcal{C}_i$ and Definition 3, we define $\theta_r = \arccos(\sqrt{\epsilon}_r) \in [0, \frac{\pi}{2}]$ as the co-latitude of REO cap, $\mathcal{C}_{i_r}$. More formally, we have

$$\begin{aligned} \mathcal{C}_{i_q} \equiv \{\mathcal{P}_j : \arccos(\mathrm{E}\left\{ \|\underline{h}_i^H \underline{h}_j\|^2 \right\}) < \theta_q\} \\ \forall\ \mathcal{P}_j\ \in\ \mathcal{S}^N \ , \end{aligned} \tag{4.6}$$

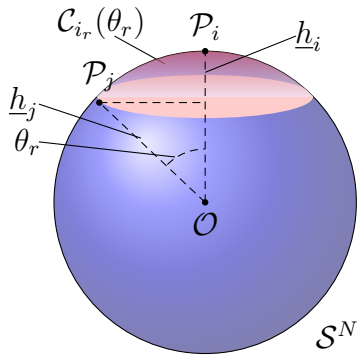

Figure 4.1: Definition of spherical cap $\mathcal{C}_{i_r}$ on the surface $\mathcal{S}^N$.

and

$$\mathcal{C}_{i_r} \equiv \{\mathcal{P}_j : \arccos(\mathrm{E}\left\{\mathrm{Re}\{\underline{h}_i^H \underline{h}_j\}^2\right\}) < \theta_r\} \quad \forall\ \mathcal{P}_j\ \in\ \mathcal{S}^N\ , \tag{4.7}$$

where $\mathcal{P}_j$ is an arbitrary point on the surface $\mathcal{S}^N$ belonging to the vector $\underline{h}_j$.

The concept of spherical caps can be related to relaxed user orthogonality. This is equivalent to vectors projected randomly onto $\mathcal{S}^N$ with a uniform density independently from another one. We define $p_\perp$ as the probability that L spherical caps of co-latitude angle θ on $\mathcal{S}^N$ have an average overlap area less than or equal to ϵ,

$$p_\perp \equiv Pr[\mathrm{E}\{V\} \leq \epsilon, \forall i \neq j \in \mathsf{A}, |\mathsf{A}| = L]. \tag{4.8}$$

Computation of $p_\perp$ is approached as a random point packing problem.

4.1 Random sphere packing formulation

Random point packing on a hyper-sphere of arbitrary dimension is a well-known problem with a wide variety of applications. It is important to differentiate between random packing and deterministic packing problems. In the context of information theory and communications Shannon famously formulated channel capacity analysis as a deterministic hyper-sphere packing problem [19]. In this analysis, non-overlapping spheres representing noisy codewords are packed into a larger spherical space whose volume is a function of signal power. Thus, capacity becomes a ratio of signal sphere volume to noise sphere volume (i.e. SNR). This problem differs from the random sphere packing problem in the respect that codeword spheres are packed at deterministic locations. In contrast, the locations of packing elements (i.e. spheres caps, etc.) in the random sphere packing problem are stochastic. Therefore, packing non-overlapping elements in the hyper-spherical space requires statistical analysis.

Existence of REO and QEO groups can be formulated as one such random packing problem. The probability of finding an ϵ-orthogonal group becomes the probability of packing L randomly placed caps with half-angle θ on $\mathcal{S}^N$ with a limited amount of average overlap. Analyzing and computing such a probability becomes increasingly challenging as L grows. The probability of packing subsequent caps depends on the placement of previous caps on $\mathcal{S}^N$. The placement of previous caps is stochastic as well. Moreover, discrete caps can take any location on the continuous space $\mathcal{S}^N$. This scenario becomes intractable very quickly.

Instead of attempting to compute the probability of packing L caps onto $\mathcal{S}^N$ directly, this quantity will be approximated by computing the mean fraction of non-overlapping caps using Theorem 1 in [39].

We define the indicator variable 1_i as

$$1_i(\theta, \mathsf{A}) = \begin{cases} 0, & \text{if } \mathcal{C}_i(\frac{\theta}{2}) \cap \mathcal{C}_j(\frac{\theta}{2}) = \emptyset \ \forall \ j \neq i; \ j = 1 \dots L \\ 1, & \text{otherwise.} \end{cases} \tag{4.9}$$

We define F_o as fraction of overlapping caps given by

$$F_o = \frac{1}{L} \sum_{i=1}^{L} 1_i(\theta, \mathsf{A}) \quad . \tag{4.10}$$

We now take the expectation of this expression in order to arrive at the expected fraction of overlapping caps in A randomly packed onto $\mathcal{S}^N$. Since 1_i is a discrete indicator variable, its expected value is simply is probability of taking value 1. Thus we have:

$$\begin{aligned} \mathrm{E}\{F_o)\} &= \frac{1}{L} \sum_{i=1}^{L} \mathrm{E}\{1_i(\theta, \mathsf{A})\} \\ &= \frac{1}{L} \sum_{i=1}^{L} Pr[1_i(\theta, \mathsf{A}) = 1]. \end{aligned} \tag{4.11}$$

For a given cap realization or placement $c_i \in \mathcal{C}_i$, 1_i will be zero if and only if we have $(L-1)$ points $\mathcal{P}_j$ chosen independently who do not belong to $\mathcal{C}_i$. The probability that $\mathcal{P}_j \notin \mathcal{C}_i$ is related to the fractional area of $\mathcal{S}^N$ that $\mathcal{C}_i$ covers. That is,

$$Pr[\mathcal{P}_j \notin \mathcal{C}_i] = 1 - 2\frac{\Omega^N(\theta)}{\Omega^N(\pi)} \ , \tag{4.12}$$

where we define $\Omega^N(\theta)$ as the area covered by a cap of colatitude θ (i.e. $\Omega^N(\pi)$ is the entire surface area of $\mathcal{S}^N$). Note the factor of two multiplied onto this term. This factor of two appears due to the fact that co-linearity of vectors in negative and

positive directions is equivalent. Since each point $\mathcal{P}_j$ is chosen independently of the other, we have

$$Pr[1_i(\theta, \mathsf{A}) = 1 \mid \mathcal{C}_i = c_i] = 1 - (1 - 2\frac{\Omega^N(\theta)}{\Omega^N(\pi)})^{L-1} \ , \tag{4.13}$$

which is independent of our choice of c_i, and thus the sum in Eq. (4.11) is independent of the user, giving us

$$\mathrm{E}\{F_o\} = 1 - (1 - 2\frac{\Omega^N(\theta)}{\Omega^N(\pi)})^{L-1} \ . \tag{4.14}$$

Thus, we can compute $p_\perp$ as

$$\begin{aligned} p_\perp &= 1 - \mathrm{E}\{F_o\} \\ &= (1 - 2\frac{\Omega^N(\theta)}{\Omega^N(\pi)})^{L-1} \ . \end{aligned} \tag{4.15}$$

While Eq. (4.15) gives us an expression for the expected fraction of intersecting caps on $\mathcal{S}^N$ as a function of θ, and L, we still must address the computation of fractional cap cover $2\frac{\Omega^N(\theta)}{\Omega^N(\pi)}$.

4.2 Fractional cap cover

Several methods of computing fractional caps are presented in this work. Conceptual examples are first presented, followed by further methods and results useful in the context of this work.

4.2.1 Geometric expressions for real 2-sphere and real 3-sphere

Fractional cap areas can be computed exactly using analytic methods for the real unit circle (2-sphere) and real unit sphere (3-sphere). We define $\Omega^N_{\mathbb{R}}(\pi)$ as the entire

surface area of the real N-sphere. The surface of the unit circle in $\mathbb{R}^2$ is simply its circumference: $\Omega^2_{\mathbb{R}}(\pi) = 2\pi$. Therefore, for the 2-sphere the fractional cap area becomes

$$2\frac{\Omega^2_{\mathbb{R}}(\theta)}{\Omega^2_{\mathbb{R}}(\pi)} = 2\frac{\theta}{\pi} \quad . \tag{4.16}$$

The surface area of the real unit sphere is easily computed adopting a spherical coordinate system in $\mathbb{R}^3$. Using conventional spherical coordinates as parameters:

$$\begin{aligned} x &= \rho\cos(\phi)\sin(\Theta) \\ y &= \rho\sin(\phi)\sin(\Theta) \\ z &= \rho\cos(\Theta) \quad , \end{aligned} \tag{4.17}$$

where Θ is the colatitude angle, ϕ is the azimuth angle, and ρ is the radius of the sphere. The differential area element on the sphere is well-known to be $dA = \rho^2\sin(\Theta)\ d\Theta\ d\phi$, where $\rho = 1$ on the unit sphere.

The total area of the unit sphere is

$$\begin{aligned} \Omega^3_{\mathbb{R}}(\pi) &= \int_0^{2\pi}\int_0^{\pi}\sin(\Theta)\ d\Theta d\phi \\ &= 4\pi, \end{aligned} \tag{4.18}$$

while the area of a cap whose cone has half-angle θ has area

$$\begin{aligned} \Omega^3_{\mathbb{R}}(\theta) &= \int_0^{2\pi}\int_0^{\theta}\sin(\Theta)\ d\Theta d\phi \\ &= 2\pi(1-\cos(\theta)) \quad . \end{aligned} \tag{4.19}$$

Therefore the fractional area of a cap in $\mathbb{R}^3$ becomes

$$2\frac{\Omega^3_{\mathbb{R}}(\theta)}{\Omega^3_{\mathbb{R}}(\pi)} = 1 - \cos(\theta) \quad . \tag{4.20}$$

While these expressions are relatively routine, they provide a concrete test case to compare other more flexible methods against.

4.2.2 Geometric approach on the real hyper-sphere

A geometric approach by [13] suggests fractional cover of a spherical cap on a real hyper-sphere of N dimensions can be realized the incomplete regularized beta function.

We observe the following equality from Eq. (2.4):

$$\mathrm{B}_{\sin^2\theta}(\frac{N+1}{2}, \frac{1}{2}) = 2\int_0^\theta \sin^N(\phi)\ d\phi \quad . \tag{4.21}$$

We will also make use of the expression for the surface area of an entire real hyper-sphere with radius ρ in terms of the Gamma function:

$$\Omega^N_{\mathbb{R}}(\rho, \pi) = \frac{2\pi^{N/2}}{\Gamma(N/2)}(\rho)^{N-1} \quad . \tag{4.22}$$

As is illustrated in [13], the area of a spherical cap in N dimensions can be calculated by integrating the surface of a sphere in $N-1$ dimensions along the arc of a great circle with radius $\rho \sin\phi$, where the arc element along the great circle is given by $\rho\ d\phi$. This integral can be expressed in terms of the Beta function given in Eq.

(2.4).

$$\begin{aligned}\Omega_{\mathbb{R}}^{N}(\rho,\theta) &= \int_0^{\theta} \Omega_{\mathbb{R}}^{N-1}(\rho\sin\phi,\pi)\ \rho d\phi \\ &= \frac{2\pi^{N-1/2}}{\Gamma(N-1/2)}(\rho)^{N-1}\int_0^{\theta}\sin^{N-2}(\phi)d\phi \\ &= \frac{1}{2}\Omega_{\mathbb{R}}^{N}(\rho,\pi)\ \mathrm{I}_{\sin^2(\theta)}\left(\frac{N-1}{2},\frac{1}{2}\right)\end{aligned} \tag{4.23}$$

Therefore, the fractional cap cover is given by the incomplete regularized Beta function:

$$\begin{aligned}2\frac{\Omega_{\mathbb{R}}^{N}(\theta)}{\Omega_{\mathbb{R}}^{N}(\pi)} &= \mathrm{I}_{\sin^2(\theta)}\left(\frac{N-1}{2},\frac{1}{2}\right) \\ &= \mathrm{I}_{1-\epsilon}\left(\frac{N-1}{2},\frac{1}{2}\right)\ ,\end{aligned} \tag{4.24}$$

where the second equality holds since, from Eqs. (4.1), (4.2) and Fig. 4.1, $\epsilon = \cos(\theta)$. The incomplete regularized Beta function is the CDF of a Beta-distributed random variable. This gives rise to a statistical rather than a geometric interpretation. By interpreting the incomplete regularized Beta function in Eq. (4.24) as a CDF, we observe that inner products of estimated channel vectors in a real space are Beta-distributed with the following shape parameters

$$\mathrm{I}_{1-\epsilon}\left(\frac{N-1}{2},\frac{1}{2}\right) = Pr[(\underline{h}_i^T\underline{h}_j)^2 \leq 1-\epsilon]. \tag{4.25}$$

4.2.3 New Statistical approach on the complex hyper-sphere

Instead of approaching the problem geometrically as in[13], we take a novel statistical approach the the problem. The advantage of pursuing a statistical approach is the ease of extension to quadratic forms in $\mathbb{C}^N$. This is particularly useful in developing expressions for fractional cap areas following from QEO and REO inner products.

Fractional cap covers following from Definitions 2 and 3 are developed in Theorems 1 and 2, respectively.

Theorem 1. *Given the cap $\mathcal{C}_{i_q}$ on $\mathcal{S}^N$ with co-latitude angle θ_q as defined by Eq. (4.6), the fraction of the total surface area of $\mathcal{S}^N$ covered by $\mathcal{C}_{i_q}$ is given by*

$$2\frac{\Omega^N(\theta_q)}{\Omega^N(\pi)} = I_{1-\epsilon_q}\bigg(N-1,1\bigg). \tag{4.26}$$

Proof. We begin by fixing $\underline{h}_i$ on $\mathcal{S}^N$, without loss of generality, in order to form the inner product with $\underline{h}_j$. We write the inner product in the following quadratic form:

$$\|\underline{h}_i^H \underline{h}_j\|^2 = \underline{h}_j^H \underline{h}_i \underline{h}_i^H \underline{h}_j. \tag{4.27}$$

This expression can be re-written in terms of real-valued augmented vectors

$$\begin{aligned} \|\underline{h}_i^H \underline{h}_j\|^2 &= \underline{\underline{h}}_j^T \underline{\underline{h}}_i \underline{\underline{h}}_i^T \underline{\underline{h}}_j \\ &= \underline{\underline{h}}_j^T \mathbf{B} \underline{\underline{h}}_j, \end{aligned} \tag{4.28}$$

where $\underline{\underline{x}} = [\mathrm{Re}\{\underline{x}\}^T \ \mathrm{Im}\{\underline{x}\}^T]^T$, $\underline{\underline{x}}^T = [\mathrm{Re}\{\underline{x}\}^T \ -\mathrm{Im}\{\underline{x}\}^T]$, and $\mathbf{B} = \underline{\underline{h}}_i \underline{\underline{h}}_i^T$ is a $2N \times 2N$ fixed matrix.

$\mathbf{B}$ can be decomposed into the sum of two outer products $\mathbf{B} = \mathbf{B}_1 + \mathbf{B}_2$, where the outer products $\mathbf{B}_1$ and $\mathbf{B}_2$ are given as

$$\mathbf{B}_1 = \begin{bmatrix} \mathrm{Re}\{\underline{h}_i\} \\ \mathrm{Im}\{\underline{h}_i\} \end{bmatrix} \begin{bmatrix} \mathbf{I}_N & 0 \\ 0 & 0 \end{bmatrix} \begin{bmatrix} \mathrm{Re}\{\underline{h}_i\}^T \ \mathrm{Im}\{\underline{h}_i\}^T \end{bmatrix},$$

$$\mathbf{B}_2 = \begin{bmatrix} \mathrm{Re}\{\underline{h}_i\} \\ \mathrm{Im}\{\underline{h}_i\} \end{bmatrix} \begin{bmatrix} 0 & 0 \\ 0 & -\mathbf{I}_N \end{bmatrix} \begin{bmatrix} \mathrm{Re}\{\underline{h}_i\}^T & \mathrm{Im}\{\underline{h}_i\}^T \end{bmatrix},$$

Where $\mathbf{I}_N$ is the $N \times N$ identity matrix. Since $\mathbf{B}_1$ and $\mathbf{B}_2$ are outer products, $\mathrm{Ra}(\mathbf{B}_1) = \mathrm{Ra}(\mathbf{B}_2) = 1$; therefore, $\mathrm{Ra}(\mathbf{B}) = 2$, where $\mathrm{Ra}(\cdot)$ is the rank operation.

Assuming both the real and imaginary parts of $\underline{h}_i$ are normalized to unity, $\mathbf{B}$ will be an idempotent matrix. Thus, by Theorem 1.5.7 [14], the inner product will be Beta-distributed, i.e.,

$$\|\underline{h}_i^H \underline{h}_j\|^2 \sim \beta(1, N-1) \tag{4.29}$$

and therefore, letting $\|\underline{h}_i^H \underline{h}_j\|^2 = V_q$ and since the CDF of a Beta-distributed variable is given by the incomplete regularized Beta function, we have

$$F_{V_q}(\epsilon_q) = \mathrm{I}_{\epsilon_q}\Big(1, N-1\Big), \tag{4.30}$$

where $F_{V_q}(\epsilon_q)$ is the CDF of V_q. We note that since $\epsilon_q = \cos(\theta_q)$, we have $\sin^2(\theta_q) = 1 - \epsilon_q$. We also remark that the CDF $F_{V_q}(1-\epsilon_q),\ \epsilon_q \in [0,1]$ is the mirror of $F_{V_q}(\epsilon_q)$. Asserting the mirroring property of the Beta distribution (see Definition 1), we have

$$2\frac{\Omega^N(\theta_q)}{\Omega^N(\pi)} = \mathrm{I}_{\sin^2(\theta_q)}\Big(N-1, 1\Big). \tag{4.31}$$

□

Theorem 2. *Given the cap $\mathcal{C}_{i_r}$ on $\mathcal{S}^N$ with co-latitude angle θ_r as defined by Eq. (4.7), the fraction of the total surface area of $\mathcal{S}^N$ covered by $\mathcal{C}_{i_r}$ is given by*

$$2\frac{\Omega^N(\theta_r)}{\Omega^N(\pi)} = I_{1-\epsilon_r}\Big(\frac{2N-1}{2}, \frac{1}{2}\Big), \tag{4.32}$$

The following proof adopts the same notation, and assumptions as the proof of Theorem 1 unless otherwise stated.

Proof. We can write the widely-linear inner product in the following quadratic form

$$\begin{aligned}\mathrm{Re}\{\underline{h}_i^H \underline{h}_j\}^2 &= \left(\begin{bmatrix}\mathrm{Re}\{\underline{h}_i\}\\ \underline{0}_N\end{bmatrix}[\mathrm{Re}\{\underline{h}_j\}^T\ \underline{0}_N^T]\right)^2 \\ &= [\mathrm{Re}\{\underline{h}_j\}^T\ \underline{0}_N^T]\mathbf{B}\begin{bmatrix}\mathrm{Re}\{\underline{h}_j\}\\ \underline{0}_N\end{bmatrix},\end{aligned} \tag{4.33}$$

where $\underline{0}_N$ is an $N \times 1$ vector of zeros. The fixed $2N \times 2N$ matrix $\mathbf{B}$ is given by the outer product

$$\mathbf{B} = \begin{bmatrix}\mathrm{Re}\{\underline{h}_i\}\\ \underline{0}_N\end{bmatrix}\begin{bmatrix}\mathrm{Re}\{\underline{h}_i\}^T\ \underline{0}_N^T\end{bmatrix}.$$

Thus, $\mathrm{Ra}(\mathbf{B}) = 1$. $\mathbf{B}$ is an idempotent matrix under the assumption that real and imaginary parts of $\underline{h}_i$ are normalized to unity. Thus, by Theorem 1.5.7 [14], the widely-linear inner product will be Beta-distributed, i.e.,

$$\mathrm{Re}\{\underline{h}_i^H \underline{h}_j\}^2 \sim \beta\left(\frac{1}{2}, \frac{2N-1}{2}\right) \tag{4.34}$$

and therefore, letting $\mathrm{Re}\{\underline{h}_i^H \underline{h}_j\}^2 = V_r$ and since the CDF of a Beta-distributed variable is given by the incomplete regularized Beta function, we have

$$F_{V_r}(\epsilon_r) = \mathrm{I}_{\epsilon_r}\left(\frac{1}{2}, \frac{2N-1}{2}\right), \tag{4.35}$$

where $F_{V_r}(\epsilon_r)$ is the CDF of V_r. We note that since $\epsilon_r = \cos(\theta_r)$, we have $\sin^2(\theta_q) =$

$1-\epsilon_r$. We also remark that the CDF $F_{V_r}(1-\epsilon_r),\ \epsilon_r \in [0,1]$ is the mirror of $F_{V_r}(\epsilon_r)$. Asserting the mirroring property of the beta distribution, we have

$$\frac{\Omega^N(\theta_r)}{\Omega^N(\pi)} = \mathrm{I}_{1-\epsilon_r}\left(\frac{2N-1}{2}, \frac{1}{2}\right). \tag{4.36}$$

□

4.2.4 Method based on Monte-Carlo integration

Contrasting analytic methods, we now propose a numerical approach to computing the fractional cover of $\mathcal{C}_i$. The proposed numerical approach computes this cover by approximating the integral over the cap using Monte-Carlo methods.

Given the N-length vector of coordinates, $\underline{C}$, that defines $\mathbb{C}^N$, the area of $\mathcal{S}^N$ can be expressed by the integral

$$\Omega^N(\pi) = \int_{\mathcal{S}^N} d\underline{C}. \tag{4.37}$$

Similarly, the area covered by the cap $\mathcal{C}_i \in \mathcal{S}^N$ can be expressed as

$$\begin{aligned} 2\Omega_N(\theta) &= 2\int_{\mathcal{C}_i} d\underline{C} \\ &= \int_{\mathcal{S}^N} \hat{1}_i(\theta, \underline{S}) d\underline{C}, \\ &\text{where:} \\ \hat{1}_i(\theta, \underline{C}) &= \begin{cases} 1, \text{ if: } |<\underline{h}_i, \underline{C}>|^2 \ \leq \cos(\theta) \\ 0, \text{ otherwise} \end{cases}. \end{aligned} \tag{4.38}$$

Note that the factor of two disappears in the second equality due to the absolute value taken on the inner product.

We can easily generate random realizations $\underline{c} \in \underline{C}$ with uniform density on $\mathcal{S}^N$ according to [41]: each element in the vector $\underline{c}$ is realized from a standard normal circular symmetric complex distribution and normalized such that it lies on $\mathcal{S}^N$. The integral for the cap area can thus be approximated as

$$2\Omega^N(\theta) \approx \frac{\Omega^N(\pi)}{Q} \sum_{\underline{c}\in\underline{C}} \hat{1}_i(\theta, \underline{c}), \tag{4.39}$$

where Q is the number of realizations $1_i(\theta, \underline{c})$ is summed over in Eq. (4.39). As the number of realizations in the arithmetic sum, Q, becomes very large, the sum approaches the integral given in Eq. (4.38), thus we have

$$2\frac{\Omega^N(\theta)}{\Omega^N(\pi)} = \lim_{Q\to\infty} \frac{1}{Q} \sum_{\underline{c}\in\underline{C}} \hat{1}_i(\theta, \underline{c}). \tag{4.40}$$

This approach is an alternative method for investigating fractional cap cover independent of methods previously presented based on the Beta Distribution.

4.2.5 Numerical and simulated results

We first provide examples that illustrate Theorems 1 and 2 comparing analytic curves to Monte-Carlo simulations. Simulated data are computed by generating random realizations uniformly on $\mathcal{S}^N$, summing those realizations which land in a given cap area. When the number of realizations in the sum become sufficiently large, the sum approximates an integral over the cap on $\mathcal{S}^N$ according to Eq. (4.40), giving a simulated fractional cap cover. Comparisons between analytic and simulated results for Theorems 1 and 2 for $N = 4$, $N = 16$ are shown in Fig. 4.2.

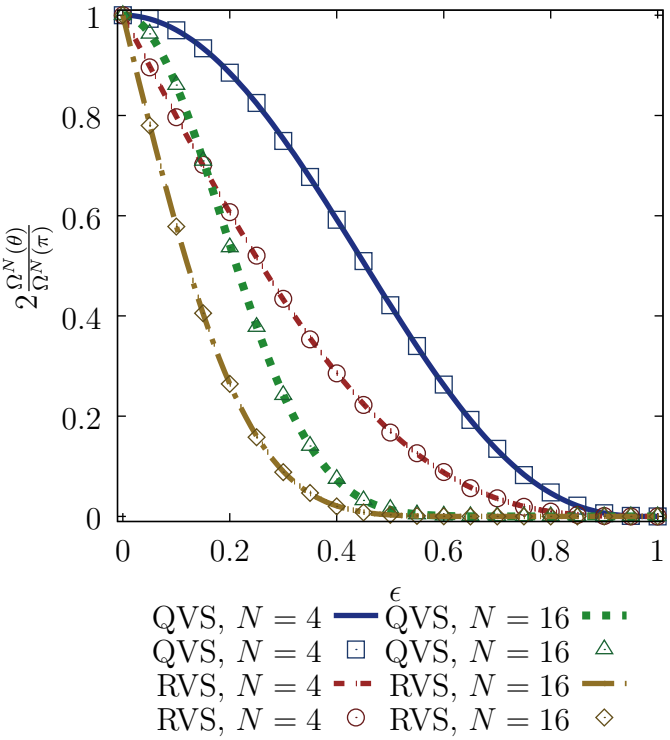

Figure 4.2: $2\frac{\Omega^N(\theta_q)}{\Omega^N(\pi)}$ and $2\frac{\Omega^N(\theta_r)}{\Omega^N(\pi)}$ given in Theorems 1 and 2 respectively, versus ϵ-orthogonality (continuous curves). 40,000-trial Monte-Carlo simulation computed according to Eq. 4.40 (discrete points).

From these curves we can make several observations. When interpreting the results plotted in Fig. 4.2, low values ϵ represent large cap sizes since the degree of orthogonality between vectors is high. Conversely, larger values ϵ correspond to smaller caps. Following from this fact, we can see lower values ϵ lead to a larger fraction of the spherical surface being covered by the cap as we expect. It is important to note that method used to generate analytic curves holds for an arbitrary value of $N \geq L$, thus allowing for an arbitrarily large choice of N. This flexibility is particularly useful for analyzing systems with a large number of antennas.

It is clear as seen from these plots that we have very close agreement between

analytic and simulated results over a variety of dimensions. Confidence intervals are omitted from plots in Fig. 4.2; however, analytic curves were found to be agreement with simulated data within this interval.

We can also observe that QVS caps corresponding to Theorem 1 cover more of the spherical surface than RVS caps corresponding to Theorem 2 for a given ϵ value. Again, this result agrees with expectations. When the QEO inner product is relaxed to be REO, we expect it to be easier to pack vectors onto the spherical surface. In order to do so, the REO caps must be smaller with respect to the QEO caps.

Furthermore, by comparing curves in Fig. 4.2, we can see that fractional area of the high-dimension case decreases more quickly as ϵ increases. This behaviour can be explained in terms of orthogonality and the increase of dimension of the hyper-sphere. A high degree of orthogonality between vectors on the hyper-sphere (low ϵ) is easier to achieve since there are more degrees of freedom present. The presence of these extra degrees of freedom make the largest difference for medium-sized caps. When ϵ is very small, the caps are so large that the sphere dimension does not matter: the cap will cover almost the entire surface. Conversely, when ϵ is large, the caps are so small that it does not matter how many dimensions or degrees of freedom we have on the sphere: the cap will cover a very small area on the surface.

The fractional cap cover results consider the placement of a single cap on $\mathcal{S}^N$. We now investigate the scenario where multiple caps are placed on the surface.

The first computation we investigate is $p_\perp$. In particular, we are interested in quantifying $p_\perp$ as a function of the number of antennas, N; the number of users in the group, L; and ϵ. The results plotted in Fig. 4.3 illustrate several scenarios. Again, analytic curves are compared to Monte-Carlo simulations.

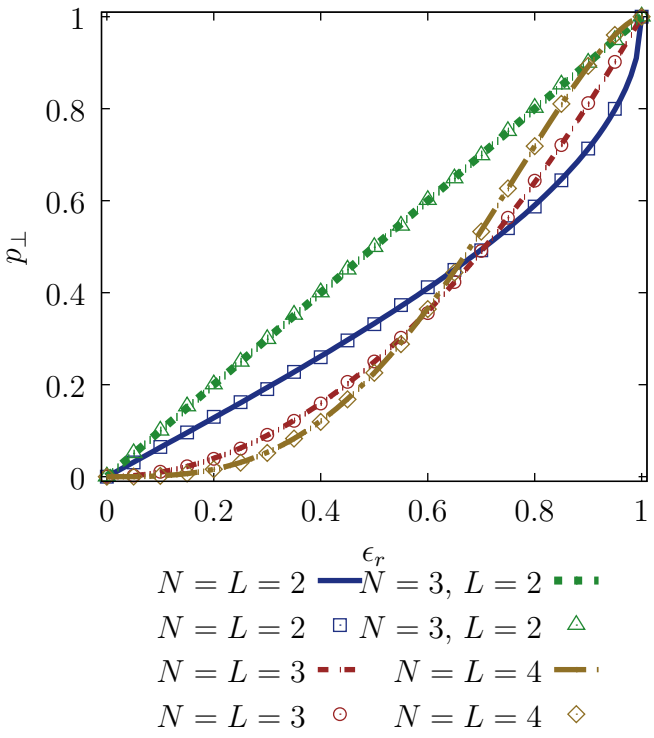

Figure 4.3: Analytic RVS $p_\perp$ plotted (continuous curves) as a function of ϵ_r. 10,000-trial Monte-Carlo simulation computed according to Eq. (4.40) (discrete points).

From Fig. 4.3, we can observe that simulated results are in agreement with analytic results for a variety of dimensions N, and numbers of caps, L. We also observe that results make sense intuitively in several regards. When the caps are large (low ϵ), then $p_\perp$ is very small: the caps are large, therefore they frequently overlap. Conversely, when the caps are small, the frequency of overlap is small: therefore, $p_\perp$ is large.

Several additional observations can also be made from the curves and data in Fig. 4.3 in comparing the $N = 3,\ L = 3$ and $N = 3,\ L = 2$ curves. We can see the first curve is always less than that belonging to the second. This is as expected since

there are more caps to be packed onto a sphere of the same degrees of freedom in the first curve relative to the second. We also observe that as N increases, so does $p_\perp$. This is illustrated by comparing $N = 2,\ L = 2$ and $N = 3,\ L = 2$ curves. The second of these curves is greater than the first. Again we note that the analytic results hold for an arbitrarily large value of N. Relatively low numbers of antennas are considered to make comparisons to simulation. In contrast to analytic results, the resources required to compute simulated results grows rapidly with the number of antennas and group size.

4.3 Dependent groups

Calculating the probability of finding a single group that satisfies our orthogonality criteria, $Pr[\mathscr{S}_\epsilon \neq \emptyset]$ as a function of $L,\ K,\ \theta(\epsilon)$ is of particular interest. In order to work up to this result, let us first consider the case that $K = L$. In this case, there is only one non-null subset of C, that is C itself.

$$Pr[\mathscr{S}_\epsilon \neq \emptyset \mid L = K] = p_\perp. \tag{4.41}$$

However, in the case that $K > L$, we must now consider multiple subsets of C. We introduce the indicator random variable 1_A which takes value 1 when $\mathsf{A} \in \mathscr{S}_\epsilon$ and 0, otherwise.

$$1_\mathsf{A} \equiv \begin{cases} 1, & \text{if } \mathsf{A} \in \mathscr{S}_\epsilon \\ 0, & \text{otherwise.} \end{cases} \tag{4.42}$$

The number of ϵ-orthogonal sets in $\mathscr{S}_\epsilon$ may be expressed as

$$\begin{aligned} K_\epsilon^{(L)} &\equiv |\mathscr{S}_\epsilon| \\ &= \sum_{\mathsf{A}\subset\mathsf{C}} 1_{\mathsf{A}}. \end{aligned} \tag{4.43}$$

We can now apply Eq. (4.41) to Eq. (4.43). We require the union of events corresponding to the existence of group sizes, j, in the range $L \leq j \leq K$,

$$Pr[\mathscr{S}_\epsilon \neq \emptyset] = \sum_{j=L}^{K} Pr[K_\epsilon^{(j)} > 0]. \tag{4.44}$$

A tractable expression to compute the argument of the sum is required. The arguments of the sum in Eq. (4.43) are not necessarily independent. This follows from the fact that the arbitrary subsets of C may have intersections. Therefore, the random variables that correspond to these sets may also be dependent. For example, consider two subsets of C, $\mathsf{A} \subset \mathsf{C}$ and $\mathsf{B} \subset \mathsf{C}$. In the case that $\mathsf{A} \cap \mathsf{B} = \emptyset$, the indicator random variables 1_{A} and 1_{B} will also be independent. However, when $\mathsf{A} \cap \mathsf{B} \neq \emptyset$, then the random variables 1_{A} and 1_{B} are dependent.

To account for this dependence in developing an accurate bound on $Pr[\mathscr{S}_\epsilon \neq \emptyset]$, the following graph-based approach will be adopted as in [12], [40]. Firstly, a graph will be generated based on the multiplication of the channel matrix and its conjugate transpose (Hermitian). The resulting square matrix is then transformed based on the channel orthogonality constraints given in Eqs. (3.10) and (3.11). This is approach taken by [12]. The transformed elements that remain in the matrix after this are then interpreted as a graph which can be used to quantify the sum given in Eq. (4.43) using the method given by [40].

Let us define $\mathbf{H}_K$ as the channel matrix whose columns are the channel vectors corresponding to the set of candidate vectors C. Therefore, $\mathbf{H}_K$ is a $N \times K$ matrix. Next let us define the $K \times K$ square matrix given by

$$\mathbf{G}_K = \mathbf{H}_K^H \mathbf{H}_K \quad . \tag{4.45}$$

At this time, take a moment to note what the elements of $\mathbf{G}_K$ represent. The diagonal elements of $\mathbf{G}_K$ are the norm of the channel estimates and, therefore, set to unity under the assumption of channel normalization. The off-diagonal elements are the inner products between the various channel vectors. Let us define

$$\Lambda = \mathfrak{T}(\mathbf{G}_K,\ \theta), \tag{4.46}$$

which transforms the matrix $\mathbf{G}_K$ into the graph Λ. The transformation $\mathfrak{T}$ operates as follows: first we draw K vertices in Λ: one for each term along the main diagonal of $\mathbf{G}_K$. Next, starting in the first row of $\mathbf{G}_K$, we compare off-diagonal elements to ϵ-orthogonal user constraints. We draw an edge between the first vertex and the vertex of a given column index if that off-diagonal element is less than ϵ. We proceed to the second row drawing edges using the same rule, skipping edges if they already exist. This process is continued for all K rows in $\mathbf{G}_K$ until all the edges in Λ are drawn.

Let us take a moment to draw connections between the graph Λ and the ϵ-orthogonal group definitions given in Eqs. (3.10) and (3.11). The number of vertices in the graph is the same as the cardinality of the set of candidate vectors $|\mathsf{C}| = K$. The collection of sets $\mathscr{S}_\epsilon$ in Eqs. (3.10) and (3.11) can be represented in Λ by forming graph $\mathscr{A}$ which is defined as the collection of $\binom{K}{L}$ L-tuples, A, on the vertices of Λ,

regardless of whether or not edges exist, then testing against ϵ. The graph interpretation can be related to 1_{A} in terms connectivity between vertices. If the L-tuple of vertices, $\mathsf{A} \in \Lambda$ is fully connected, then $1_{\mathsf{A}} = 1$, otherwise $1_{\mathsf{A}} = 0$. Moreover, $\mathscr{A}$ can also be interpreted as a graph representing dependence between L-tuples. Each of the L-tuples $\mathsf{A} \in \mathscr{A}$ is a vertex. Vertices in $\mathscr{A}$ are connected with an edge if they share a common element between tuples.

It is important to note before proceeding that 1_{A} is a Bernoulli-distributed random variable, which takes value 1 with probability $p_{\perp}$. A requirement of using the approach in [40] is that 1_{A} and 1_{B} be independent so long as there is no intersections between the sets A and B. This may appear to be a redundant statement; however, if the random variables upon which 1_{A} and 1_{B} depend are correlated, this condition does not hold. However, since we assume independence between channel estimates, the assumption holds.

Two upper bounds are given in [40]. First, according to Theorem 2.1, [40]:

$$Pr[K_{\epsilon}^{(L)} \leq \mathrm{E}\{K_{\epsilon}^{(L)}\} - x] \leq \exp\left(\frac{-2x^2}{\chi^*(\mathscr{A})|\mathscr{A}|}\right) \ ; \tag{4.47}$$

second, according to Corollary 2.4 [40]:

$$Pr[K_{\epsilon}^{(L)} \leq \mathrm{E}\{K_{\epsilon}^{(L)}\} - x] \leq \exp\left(\frac{-8x^2}{25\chi^*(\mathscr{A})p_{\perp}|\mathscr{A}|}\right) \ , \tag{4.48}$$

where $\chi^*(\mathscr{A})$ is the fractional chromatic number of the dependency graph $\mathscr{A}$.

In our case, we are particularly interested in the case $Pr[K_{\epsilon}^{(L)} = 0]$ corresponding to Eq. (4.44). In order to arrive at this result we manipulate the expressions

given in Eqs. (4.47),(4.48) as follows: first, we notice that the sum of Bernoulli random variables results in a binomial distribution for $K_\epsilon^{(l)}$. The mean of the binomial distribution, regardless of dependence in the sum, is given by

$$\begin{aligned} \mathrm{E}\{K_\epsilon^{(L)}\} &= |\mathscr{A}|p_\perp \\ &= \binom{K}{L}p_\perp. \end{aligned} \tag{4.49}$$

It can be shown similarly to [40] Example 4, that so long as the conditions of independence hold as described above, $\chi^*(\mathscr{A})$ can be bounded as:

$$\chi^*(\mathscr{A}) \leq \chi^*(\Lambda) \leq \frac{\binom{K}{L}}{\lfloor \frac{K}{L} \rfloor} \quad . \tag{4.50}$$

Thus, following from Eq. (4.47):

$$\begin{aligned} Pr[K_\epsilon^{(L)} = 0] &\leq Pr[K_\epsilon^{(L)} \leq 0] \\ &\leq \exp\left(\frac{-2p_\perp^2\binom{K}{L}^2}{\frac{\binom{K}{L}}{\lfloor \frac{K}{L} \rfloor}\binom{K}{L}}\right) \\ &= \exp\left(-2p_\perp^2 \lfloor \frac{K}{L} \rfloor\right). \end{aligned} \tag{4.51}$$

Similarly, following from Eq. (4.48):

$$\begin{aligned} Pr[K_\epsilon^{(L)} = 0] &\leq Pr[K_\epsilon^{(L)} \leq 0] \\ &\leq \exp\left(\frac{-8p_\perp^2\binom{K}{L}^2}{25\frac{\binom{K}{L}}{\lfloor \frac{K}{L} \rfloor}p_\perp\binom{K}{L}}\right) \\ &= \exp\left(\frac{-8p_\perp \lfloor \frac{K}{L} \rfloor}{25}\right). \end{aligned} \tag{4.52}$$

Finally to guarantee an upper bound on $Pr[K_\epsilon^{(L)} = 0]$, we have:

$$Pr[K_\epsilon^{(L)} = 0] \leq \exp\left(- \max\left\{ \frac{8p_\perp \lfloor \frac{K}{L} \rfloor}{25}, 2p_\perp^2 \lfloor \frac{K}{L} \rfloor \right\} \right) \quad . \tag{4.53}$$

Therefore, following from Eqs. (4.43),(4.44),(4.53), we can write the lower bound on $Pr[\mathscr{S}_\epsilon \neq \emptyset]$ as

$$\begin{aligned} &Pr[\mathscr{S}_\epsilon \neq \emptyset] \geq \\ &\qquad \sum_{j=L}^{K} (1 - \exp\left(- \max\left\{ \frac{8p_\perp \lfloor \frac{K}{j} \rfloor}{25}, 2p_\perp^2 \lfloor \frac{K}{j} \rfloor \right\} \right)). \end{aligned} \tag{4.54}$$

Eq. (4.54) is significant in that it gives us a bounding function that describes the probability of finding a ϵ-orthogonal group of users in terms of key parameters L, K, N, and ϵ.

4.3.1 Numerical and simulated results

Now that results have been extended to consider multiple caps on a spherical surface, we seek to extend the numerical results to consider the scenario where this group of caps is selected from a pool of K candidates. We consider the scenario where $L = 4$, $K = 30$. A large number of candidate users is assumed to reflect a densely deployed wireless network. Analytic results from Eq. (4.54) are compared to Monte-Carlo simulations.

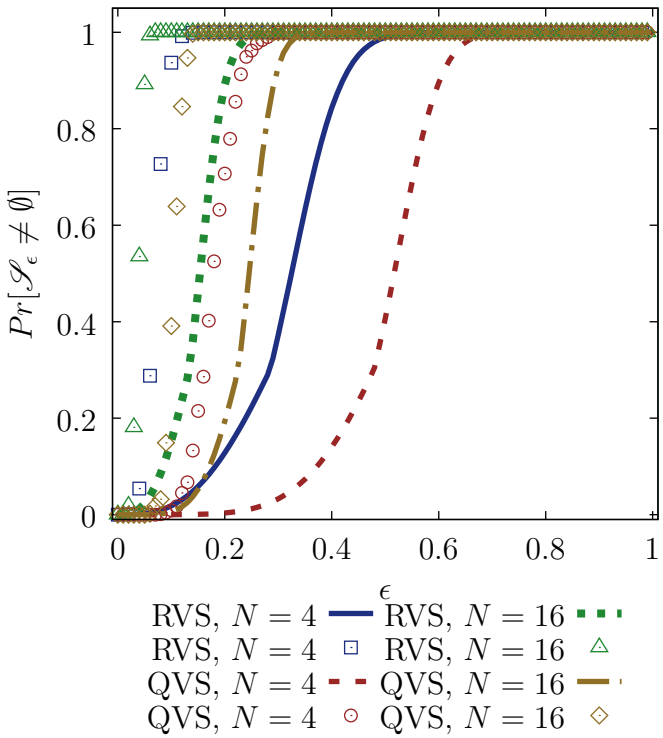

Figure 4.4: $Pr[\mathscr{S}_\epsilon \neq \emptyset]$ for $L = 4$, $K = 30$ plotted as a function of ϵ. Continuous analytic curves are a lower-bound on group existence probability given by Eq. (4.54). 80,000-trial Monte-Carlo simulation computed according to Eq. (4.40) (discrete points).

Fig. 4.4 reiterates some of the observations made in Fig. 4.3. Again, we observe a higher $Pr[\mathscr{S}_\epsilon \neq \emptyset]$ for RVS than QVS. This is unsurprising since the analytic curves in Fig. 4.4 are a function of analytic curves presented previously in Figs. 4.2 and 4.3. Consider a constant group existence probability of $Pr[\mathscr{S}_\epsilon \neq \emptyset] = 0.5$ for the purpose of quantitative RVS-QVS comparisons. From Fig. 4.4 we observe $\epsilon_q = 0.53$ and $\epsilon_r = 0.34$ for QVS and RVS,respectively, to achieve the desired group existence probability of 0.5, for $N = 4$ transmit antennas. Similarly we observe $\epsilon_q = 0.23$ and $\epsilon_r = 0.12$ for $N = 16$. It is clear that the additional degrees of freedom from more transmit antennas allows for more strict orthogonality between users for a given

group existence probability. It is also clear the the RVS criterion is able to achieve better orthogonality between users than the QVS criterion for a given group existence probability and number of antennas. Again, we note that the analytic results hold for an arbitrarily large value of N. Relatively low numbers of antennas are considered to make comparisons to simulation. In contrast to analytic results, the computational resources required for simulated results grow rapidly with the number of antennas and group size.

From Fig. 4.4, we can see that there are several factors that impact how tight Eq. (4.54) bounds simulated data. We observe that the analytic and simulated curve agree more closely for $N = 16$ than for $N = 4$, and more closely for RVS than for QVS. It is also important to note that results in [40] used in Eq. (4.54) assume a large amount of independence between arguments of the sum. Therefore, for the bound to be tight, there must relatively few users common between candidate groups. Thus, as in [40], we require $K >> L$ (i.e., the candidate groups will have a large amount of statistical independence). This criterion is well-suited to the scenario we are interested in. In a densely deployed scenario, it is likely the candidate pool will be large. We are also interested in modelling systems with many antennas; in this scenario, the analytic bound is tighter and the system can support a large group size.

4.4 Chapter summary

The spherical abstraction and associated methods presented in this chapter provide quantitative insights into the probability of ϵ-orthogonal group existence in the context of QVS and RVS models. Results illustrate trade-offs in terms of system and environmental parameters including the number of antennas at the transmitter, number

of users in the group, and number of candidates (density of users in the environment). Analytic results incorporate a new statistical approach to computing fractional cap area in a random sphere packing context. The analytic approach developed scales well to systems with a large number of antennas. Simulated results utilize a novel approach abstracting Monte-Carlo integration to the spherical space of the random packing problem. The results generated in this chapter provide a deeper understanding of orthogonality criteria that underpin many practical user selection algorithms and enable further system performance analysis.

Chapter 5

SDMA Beamforming

Performance of the MIMO system depends on the specific beamforming scheme adopted by the system. Several linear beamforming schemes are investigated to better understand the trade-offs associated particular schemes. Five linear beamforming schemes are considered: maximum-ratio transmission beamforming (MRTBF), widely linear MRTBF (WL-MRTBF), zero-forcing beamforming (ZFBF), regularized ZFBF (RZFBF)[42, 43] , and widely linear RZFBF (WL-RZFBF). Each of these schemes are first presented and discussed. Following this discussion, a subset of these schemes are analyzed jointly with ϵ-orthogonal group criteria. The QEO and REO groups considered previously use MRT and RZFBF while the REO groups use WL-MRTBF and WL-RZFBF. The objective of this joint analysis is to gain insight into the interaction between ϵ-orthogonality and beamforming. MRTBF and RZFBF are considered in the context of the QVS model. Similarly, motivated by [28, 29], WL-MRTBF and WL-RZFBF are considered in the context of the RVS model.

5.1 MRTBF and WL-MRTBF

Consideration of MRTBF is motivated by relatively low computational complexity and maximization of SNR. While MRTBF neglects interference, the objective constraining user orthogonality is interference mitigation. In this sense, the analysis illustrates how interference-mitigating user orthogonality constraints can be used to support a low-complexity beamforming scheme that is optimal in the SNR sense.

We define the $L \times N$ MRT beamforming matrix $\mathbf{W}^{MRT}$. We also define the i^{th} row of $\mathbf{W}^{MRT}$ as the $1 \times N$ beamforming row vector $\underline{w}_i^{MRT}$ for the i^{th} user in the group. Maximal signal gain is achieved when

$$\mathbf{W}^{MRT} = \mathbf{H}^H, \tag{5.1}$$

by the Cauch-Schwarz inequality [25]. As shown by [28], the matrix $\mathbf{W}_{MRT}$ is the same for both MRTBF and WL-MRTBF. Although the beamforming vector is common between these schemes, WL-MRTBF is advantageous by being able to support concurrent transmission to groups of size $L \leq 2N$, while MRTBF only supports groups of size $L \leq N$ (see Appendix [28]).

We assume a total of P_{MRT} Watts is available at the transmitter. The total transmit power is given by

$$\begin{aligned} P_{MRT} &= \mathrm{Tr}(\mathbf{W}^{MRT}(\mathbf{W}^{MRT})^H) \\ &= \sum_{i=1}^{L} \|\underline{w}_i^{MRT}\|^2 \\ &= L, \end{aligned} \tag{5.2}$$

where each user experiences an assumed equal-gain channel according to the system model assumed in Chapter 3. Therefore, uniform power allocation is implicitly built into channel assumptions for ϵ-orthogonal user selection MRTBF.

5.2 RZFBF

MRTBF is an optimal beamforming scheme in the SNR sense; it neglects interference. Similarly, ZFBF is optimal in the SIR sense; it neglects noise. In contrast ZFBF requires large amounts of power for poorly-conditioned scenarios [32, 42]. Transmit beamforming that is optimal in the SINR sense is a well-known problem, whose performance is achieved by MMSEBF[25]. The RZFBF scheme [42, 43] is also similar to minimum-mean squared error beamforming (MMSEBF) scheme that is optimal in the SINR sense. MMSEBF requires an estimate of the noise power or SNR. Based on this estimate, the beamformer places emphasis on mitigating noise or interference corruption of the received signal. MMSEBF does not necessarily assign transmit power uniformly for each user; rather, the transmit power is optimally allocated such that a function of SINR is maximized. Accurately estimating noise power with low complexity is a challenging problem [26]. RZFBF substitutes this estimate for a scalar regularization factor chosen at the transmitter. This factor ought to be chosen based on whether a noise-limited or interference-limited environment is expected. However, it is not a strict estimate of noise variance as in MMSEBF, nor is RZFBF optimal in the same sense. The RZFBF scheme is motivated by its relative simplicity. Sub-optimal uniform power allocation is assumed for RZFBF for the sake of simplicity: optimal power allocation is an NP-hard problem [44].

Motivated by the SINR-optimal beamforming structure in Problem 2 [25] and [42]

we present an expression for the $L \times N$ RZF beamforming matrix, $\mathbf{W}^{RZF}$. We assume that we are given channel matrix $\mathbf{H}$, and scalar regularization factor τ. The RZFBF is given by

$$\mathbf{W}^{RZF} = (\mathbf{I}_L + \frac{\mathbf{H}^H\mathbf{H}}{\tau})^{-1}\mathbf{H}^H, \tag{5.3}$$

where $\mathbf{I}_N$ is the $N \times N$ identity matrix. We also note that $N \geq L$, and therefore the Moore Penrose pseudo-inverse in Eq. (5.3) is taken as the left inverse.

The term τ acts as a scaling factor between MRTBF and ZFBF schemes. Let us consider Eq. (5.3) in a low SNR scenario. If we expect to be in a low SNR environment, we choose a large value for τ . Thus we have

$$\begin{aligned} \lim_{\tau \to \infty} \mathbf{W}^{RZF} &= \mathbf{H}^H \\ &= \mathbf{W}^{MRT}. \end{aligned} \tag{5.4}$$

Eq. (5.4) illustrates that when the SNR becomes low, RZFBF converges to an MRTBF, which neglects interference to compensate for the purely noise-limited channel. Conversely, when SNR is high, a small value of τ is chosen, and the RZFBF converges to the ZFBF, which neglects noise to compensate for the purely interference-limited channel.

The transmit power of MRTBF is constrained (and finite). This power constraint does not hold for RZFBF and ZFBF since $\mathbf{W}^{RZF}$ and $\mathbf{W}^{ZF}$ involve inverting matrices which may have determinants close or equal to 0, causing the transmit power required to realize these beamforming matrices to be very large. Thus, assuming we have a total transmit power P_{RZF} available, we hold $\mathbf{W}^{RZF}$ subject to

$$\mathrm{Tr}(\mathbf{W}^{RZF}(\mathbf{W}^{RZF})^H) \leq P_{RZF}. \tag{5.5}$$

We define the $1 \times N$ row vector $\underline{w}_{i_{RZF}}$ as the i^{th} row of $\mathbf{W}^{RZF}$, which belongs to the i^{th} user in the ϵ-orthogonal group. We assume uniform power allocation, allocating a magnitude of $\sqrt{\frac{P_{RZF}}{L}}$ to each vector. Therefore, we have the normalized beamforming vector

$$\widetilde{\underline{w}}_i^{RZF} \equiv \sqrt{\frac{P_{RZF}}{L}} \frac{\underline{w}_i^{RZF}}{\|\underline{w}_i^{RZF}\|} \tag{5.6}$$

In summary, under uniform power allocation we express the power constraint as

$$P_{RZF} = \sum_{i=1}^{L} \|\widetilde{\underline{w}}_i^{RZF}\|^2. \tag{5.7}$$

5.3 WL-RZFBF

In contrast to MRTBF, ZFBF and MMSEBF has different beamforming matrices depending on whether a widely-linear or conventional variant of the beamforming scheme is assumed [28]. Motivated by this result, we develop a widely-linear variant of regularized zero-forcing beamforming (WL-RZFBF). We distinguish between WL-RZFBF and widely-linear MMSEBF (WL-MMSEBF) in the sense that WL-RZFBF does not achieve optimal WL-MMSE performance, although it is based on the same principles and structure as the MMSEBF.

Based on the optimal WL-MMSEBF structure developed in [28] and the RZFBF structure from [42], we define the WL-RZFBF beamforming matrix as

$$\mathbf{W}^{WLRZF} = (\mathbf{I}_L + \frac{\mathrm{Re}\{\mathbf{H}^H\mathbf{H}\}}{\tau})^{-1}\mathbf{H}^H. \tag{5.8}$$

Uniform power allocation for WL-RZFBF is performed using a similar method as for RZFBF.

5.4 Joint analysis of beamforming and user orthogonality for maximum interference power case

A primary objective of this work is to investigate the interaction between constraining user orthogonality and beamforming. In order to do so, we focus on the special case of maximum interference power allowed by user orthogonality constraints. In this special case, the interference power for each user in the group is assigned the same maximum value on a power basis. This scenario is of particular interest for several reasons. Assignment of maximum interference power to each user in the group allows us to characterize the maximal impact of user selection algorithms in a power sense. The analysis of this scenario provides a conservative reference, since interference power is held to a maximum value, to compare against practical user selection algorithm performance. In this special case, we have implicitly set interference power for each user to the same value. Assuming the system implements a practical user selection algorithm, uniform interference power amongst users is reasonable. It is probable that a user selection algorithm will distribute interference on a somewhat uniform basis amongst users in the group, thus ensuring fairness and avoiding spatial clustering of users.

We define G_{sig} and G_{int}, as the signal and interference beamforming gains a given user in the group, respectively in the maximum interference power scenario. No specific beamforming scheme is assumed for G_{sig} and G_{int}. When a system adopts beamforming scheme x, we adopt the following notation for the ensuing analysis: $G_{sig} = G_{sig}^{x}$, $G_{int} = G_{int}^{x}$, $\mathbf{W} = \mathbf{W}^{x}$, and $\underline{w}_i = \underline{w}_i^{x}$. Interference and signal gain will be analyzed for RZFBF, WL-RZFBF, then extended to the MRTBF using Eq. (5.4).

5.4.1 RZFBF analysis

Given an $N \times L$ matrix of channel vectors $\mathbf{H}$ held subject to QEO user selection, define

$$\mathbf{H}_L^2 \equiv \begin{bmatrix} 1 & \sqrt{\epsilon_q} & \cdots & \sqrt{\epsilon_q} \\ \sqrt{\epsilon_q} & 1 & \cdots & \sqrt{\epsilon_q} \\ \vdots & \ddots & \ddots & \vdots \\ \sqrt{\epsilon_q} & \sqrt{\epsilon_q} & \cdots & 1 \end{bmatrix}, \tag{5.9}$$

where the off diagonal elements of $\mathbf{H}_L^2$ are $\underline{h}_i^H \underline{h}_j$. The maximum average interference power allowed by the QEO user orthogonality constraint in Eq. (3.10) yields $\mathrm{E}\{\|\underline{h}_i^H \underline{h}_j\|^2\} = \epsilon_q$.

Given the regularization factor, τ, define the matrix

$$\mathbf{G}_L^2 \equiv \left(\mathbf{I}_L + \frac{\mathbf{H}_L^2}{\tau}\right)^{-1} = \begin{bmatrix} \Xi & \xi & \cdots & \xi \\ \xi & \Xi & \cdots & \xi \\ \vdots & \ddots & \ddots & \vdots \\ \xi & \xi & \cdots & \Xi \end{bmatrix}, \tag{5.10}$$

where $\mathbf{I}_L$ is the $L \times L$ identity matrix.

Define the power-normalizing factor

$$P_q \equiv \sqrt{(\mathbf{G}_L^2 \mathbf{H}^H \mathbf{H} (\mathbf{G}_L^2)^H)_{i,i}}, \tag{5.11}$$

where $(\mathbf{X})_{i,i}$ denotes the i^{th} diagonal element of the matrix $\mathbf{X}$.

Proposition 1. *Given* $\boldsymbol{W}_{RZF} = (\boldsymbol{I}_L + \frac{\boldsymbol{H}^H \boldsymbol{H}}{\tau})^{-1} \boldsymbol{H}^H$ *and QEO user constraints, the*

RZFBF signal and interference gains are, respectively,

$$G_{sig}^{RZF} = \frac{1}{P_q}\sqrt{\frac{P_{RZF}}{L}}\frac{\tau\big(\epsilon_q(1-L)+\sqrt{\epsilon_q}(L-2)+\tau+1\big)}{(1+(L-1)\sqrt{\epsilon_q}+\tau)(1-\sqrt{\epsilon_q}+\tau)} \tag{5.12}$$

and

$$G_{int}^{RZF} = \frac{1}{P_q}\sqrt{\frac{P_{RZF}}{L}}\frac{(\tau)^2\sqrt{\epsilon_q}}{(1+(L-1)\sqrt{\epsilon_q}+\tau)(1-\sqrt{\epsilon_q}+\tau)}. \tag{5.13}$$

Proof. The eigen decomposition of $\mathbf{H}_L^2$ is

$$\mathbf{H}_L^2 = \sum_{i=1}^{L} \lambda_i \underline{e}_i \underline{e}_i^H \quad , \tag{5.14}$$

where $\underline{e}_i$ is the $L \times 1$ eigenvector of $\mathbf{H}_L^2$ corresponding to eigenvalue λ_i. We let $\underline{e}_1 = \frac{1}{\sqrt{L}}\underline{1}_L$, where $\underline{1}_L$ is an $L \times 1$ vector whose elements are each unity. Thus, Eq.(5.14) becomes

$$\mathbf{H}_L^2 = (1-\sqrt{\epsilon_q})\mathbf{I}_L + \sqrt{\epsilon_q}\underline{1}_L\underline{1}_L^H \quad . \tag{5.15}$$

The first rank-L term in this sum has L eigevalues $= (1-\sqrt{\epsilon_q})$ while the second rank-1 term has a single eigenvalue $= L\sqrt{\epsilon_q}$. Thus, the eigenvalues of $\mathbf{H}_L^2$ are clearly

$$\begin{aligned} \lambda_1 &= (1-\sqrt{\epsilon_q}) + L\sqrt{\epsilon_q} = 1 + (L-1)\sqrt{\epsilon_q} \quad , \\ \lambda_2 &= \lambda_3 \ldots = \lambda_L = 1 - \sqrt{\epsilon_q} \quad . \end{aligned} \tag{5.16}$$

The eigen decomposition of $\mathbf{G}_L^2$ is

$$\mathbf{G}_L^2 = \sum_{i=1}^{L} \frac{\tau}{\lambda_i + \tau} \underline{e}_i \underline{e}_i^H \quad , \tag{5.17}$$

where the eigenvectors and values are the same as those given in Eq. (5.14). Therefore, we have

$$\mathbf{G}_L^2 = \frac{\tau}{1+(L-1)\sqrt{\epsilon_q}+\tau}\underline{e}_1\underline{e}_1^H + \sum_{i=2}^{L}\frac{\tau}{1-\sqrt{\epsilon_q}+\tau}\underline{e}_i\underline{e}_i^H \quad . \tag{5.18}$$

The collection of eigenvectors $\underline{e}_i \ \forall i = 1,\ 2 \dots\ L$ form an ortho-normal set by definition. Thus, $\mathbf{I}_L = \sum_{i=1}^{L}\underline{e}_i\underline{e}_i^H$, which implies $\sum_{i=2}^{N}\underline{e}_i\underline{e}_i^H = \mathbf{I}_L - \underline{e}_1\underline{e}_1^H$. Therefore, we can re-write the decomposition in Eq. (5.18) as

$$\begin{aligned}\mathbf{G}_L^2 &= \frac{\tau}{L(1+(L-1)\sqrt{\epsilon_q}+\tau)}\underline{1}_L\underline{1}_L^H + \frac{\tau}{1-\sqrt{\epsilon_q}+\tau}\mathbf{I}_L - \frac{\tau}{L(1-\sqrt{\epsilon_q}+\tau)}\underline{1}_L\underline{1}_L^H \\ &= \frac{\tau\underline{1}_L\underline{1}_L^H}{L}\left(\frac{1}{(1+(L-1)\sqrt{\epsilon_q}+\tau)} - \frac{1}{1-\sqrt{\epsilon_q}+\tau}\right) + \frac{\tau}{1-\sqrt{\epsilon_q}+\tau}\mathbf{I}_L \\ &= \frac{-\tau\sqrt{\epsilon_q}\underline{1}_L\underline{1}_L^H}{(1+(L-1)\sqrt{\epsilon_q}+\tau)(1-\sqrt{\epsilon_q}+\tau)} + \frac{\tau}{1-\sqrt{\epsilon_q}+\tau}\mathbf{I}_L.\end{aligned} \tag{5.19}$$

From the definition of $\mathbf{G}_L^2$, we have

$$\Xi = \frac{\tau(1+(L-2)\sqrt{\epsilon_q}+\tau)}{(1+(L-1)\sqrt{\epsilon_q}+\tau)(1-\sqrt{\epsilon_q}+\tau)}, \tag{5.20}$$

and

$$\xi = \frac{-\tau\sqrt{\epsilon_q}}{(1+(L-1)\sqrt{\epsilon_q}+\tau)(1-\sqrt{\epsilon_q}+\tau)}. \tag{5.21}$$

We define the $1 \times N$ row vector $\underline{g}_i$ as the i^{th} row of the product $\mathbf{G}_L^2\mathbf{H}^H$.

We also define the $1 \times N$ row vector $\underline{g}_i$ as the i^{th} row of the product $\mathbf{G}_L^2\mathbf{H}^H$. Thus, in the context of the maximal allowable interference power case, the signal gain is

given by

$$\begin{aligned} G_{sig}^{RZF} &= \mathrm{E}\left\{ \frac{1}{P_q}\sqrt{\frac{P_{RZF}}{L}}\underline{g}_i\underline{h}_i \right\} \\ &= \frac{1}{P_q}\sqrt{\frac{P_{RZF}}{L}}(\Xi\ \|\underline{h}_i\|^2 + \xi\ \mathrm{E}\{\sum_{l=1\neq i}^{L}\sum_{k=1}^{N} h_{lk}^* h_{ik}\}) \\ &= \frac{1}{P_q}\sqrt{\frac{P_{RZF}}{L}}(\Xi + \xi(L-1)\sqrt{\epsilon_q}) \\ &= \frac{1}{P_q}\sqrt{\frac{P_{RZF}}{L}}\frac{\tau(\epsilon_q(1-L)+\sqrt{\epsilon_q}(L-2)+\tau+1)}{(1+(L-1)\sqrt{\epsilon_q}+\tau)(1-\sqrt{\epsilon_q}+\tau)}. \end{aligned} \tag{5.22}$$

Similarly, the interference gain is given by

$$\begin{aligned} G_{int}^{RZF} &= \mathrm{E}\left\{ \frac{1}{P_q}\sqrt{\frac{P_{RZF}}{L}}\underline{g}_i\underline{h}_j \right\}\ \forall\ j\neq i = 1,\ 2, \dots L \\ &= \frac{1}{P_q}\sqrt{\frac{P_{RZF}}{L}}(\Xi\ \mathrm{E}\{\underline{h}_i^H\underline{h}_j\} + \xi\ \mathrm{E}\{\sum_{l=1\neq i}\sum_{k=1}^{N} h_{lk}^* h_{jk}\}) \\ &= \frac{1}{P_q}\sqrt{\frac{P_{RZF}}{L}}(\Xi\sqrt{\epsilon_q} + \xi(1+(L-2)\sqrt{\epsilon_q}) \\ &= \frac{1}{P_q}\sqrt{\frac{P_{RZF}}{L}}\frac{(\tau)^2\sqrt{\epsilon_q}}{(1+(L-1)\sqrt{\epsilon_q}+\tau)(1-\sqrt{\epsilon_q}+\tau)}. \end{aligned} \tag{5.23}$$

□

5.4.2 MRTBF analysis

RZFBF converges to MRTBF as $\tau \to \infty$ according to Eq (5.4). From Proposition 1 we have

$$\begin{aligned} G_{sig}^{MRT} &= \lim_{\tau\to\infty} G_{sig}^{RZF} \\ &= \frac{(\tau)^2}{(\tau)^2} \\ &= 1. \end{aligned} \tag{5.24}$$

Similarly, from Proposition 1, Eq. (5.13) we have

$$\begin{aligned} G_{int}^{MRT} &= \lim_{\tau\to\infty} G_{int}^{RZF} \\ &= \frac{\sqrt{\epsilon_q}(\tau)^2}{(\tau)^2} \\ &= \sqrt{\epsilon_q}. \end{aligned} \tag{5.25}$$

5.4.3 WL-RZFBF analysis

Given an $N \times L$ matrix $\mathbf{H}$ of channel vectors held subject to REO user selection, define

$$\mathrm{Re}\{\mathbf{H}_L^2\} \equiv \begin{bmatrix} 1 & \sqrt{\epsilon_r} & \cdots & \sqrt{\epsilon_r} \\ \sqrt{\epsilon_r} & 1 & \cdots & \sqrt{\epsilon_r} \\ \vdots & \ddots & \ddots & \vdots \\ \sqrt{\epsilon_r} & \sqrt{\epsilon_r} & \cdots & 1 \end{bmatrix}, \tag{5.26}$$

where the off diagonal elements of $\mathbf{H}_L^2$ are $\mathrm{Re}\{\underline{h}_i^H \underline{h}_j\}$. The maximum average interference power allowed by the REO user orthogonality constraint in Eq. (3.11) yields $\mathrm{E}\{\mathrm{Re}\{\underline{h}_i^H \underline{h}_j\}^2\} = \epsilon_r$.

Given the regularization factor, τ, define the matrix

$$\mathrm{Re}\{\mathbf{G}_L^2\} \equiv \left(\mathbf{I}_L + \frac{\mathrm{Re}\{\mathbf{H}_L^2\}}{\tau}\right)^{-1} = \begin{bmatrix} \Xi_r & \xi_r & \cdots & \xi_r \\ \xi_r & \Xi_r & \cdots & \xi_r \\ \vdots & \ddots & \ddots & \vdots \\ \xi_r & \xi_r & \cdots & \Xi_r \end{bmatrix}, \tag{5.27}$$

where $\mathbf{I}_L$ is the $L \times L$ identity matrix. Define the power-normalizing factor

$$P_r = \sqrt{(\mathrm{Re}\{\mathbf{G}_L^2\}\mathbf{H}^H\mathbf{H}(\mathrm{Re}\{\mathbf{G}_L^2\})^H)_{i,i}}, \tag{5.28}$$

Proposition 2. *Given* $\boldsymbol{W}_{WLRZF} = (\boldsymbol{I}_L + \frac{Re\{\boldsymbol{H}^H\boldsymbol{H}\}}{\tau})^{-1}\boldsymbol{H}^H$ *and REO user constraints, the WL-RZFBF signal and interference gains are, respectively,*

$$G_{sig}^{WLRZF} = \frac{1}{P_r}\sqrt{\frac{P_{WLRZF}}{L}}\frac{\tau(\sqrt{\epsilon_r}\sqrt{\epsilon_q}(1-L)+\sqrt{\epsilon_r}(L-2)+\tau+1)}{(1+(L-1)\sqrt{\epsilon_r}+\tau)(1-\sqrt{\epsilon_r}+\tau)} \tag{5.29}$$

and

$$G_{int}^{WLRZF} = \frac{1}{P_r}\sqrt{\frac{P_{WLRZF}}{L}}\frac{\tau((1+\tau)\sqrt{\epsilon_q}-\sqrt{\epsilon_r})}{(1+(L-1)\sqrt{\epsilon_r}+\tau)(1-\sqrt{\epsilon_r}+\tau)}. \tag{5.30}$$

Proof. Substituting $\mathrm{Re}\{\mathbf{H}_L^2\}$, $\mathrm{Re}\{\mathbf{G}_L^2\}$ for $\mathbf{H}_L^2$, $\mathbf{G}_L^2$ in the proof of Proposition 1 and following the same method to Eqs. (5.20) and (5.21), we have

$$\Xi_r = \frac{\tau(1+(L-2)\sqrt{\epsilon_r}+\tau)}{(1+(L-1)\sqrt{\epsilon_r}+\tau)(1-\sqrt{\epsilon_r}+\tau)}, \tag{5.31}$$

and

$$\xi_r = \frac{-\tau\sqrt{\epsilon_r}}{(1+(L-1)\sqrt{\epsilon_r}+\tau)(1-\sqrt{\epsilon_r}+\tau)}. \tag{5.32}$$

We define the $1\times N$ row vector $\underline{g}_i$ as the i^{th} row of the product $\mathrm{Re}\{\mathbf{G}_L^2\}\mathbf{H}^H$. Therefore, in the context of the maximal allowable interference power case, the signal gain is

given by

$$\begin{aligned} G_{sig}^{WLRZF} &= \mathrm{E}\left\{ \frac{1}{P_r}\sqrt{\frac{P_{WLRZF}}{L}}\underline{g}_i\underline{h}_i \right\} \\ &= \frac{1}{P_r}\sqrt{\frac{P_{WLRZF}}{L}}(\Xi_r \ \|\underline{h}_i\|^2 + \xi_r \ \mathrm{E}\{\sum_{l=1\neq i}^{L}\sum_{k=1}^{N} h_{lk}^* h_{ik}\}) \\ &= \frac{1}{P_r}\sqrt{\frac{P_{WLRZF}}{L}}(\Xi_r + \xi_r(L-1)\sqrt{\sqrt{\epsilon_r}}) \\ &= \frac{1}{P_r}\sqrt{\frac{P_{WLRZF}}{L}}\frac{\tau(\sqrt{\epsilon_r}\sqrt{\epsilon_q}(1-L)+\sqrt{\epsilon_r}(L-2)+\tau+1)}{(1+(L-1)\sqrt{\epsilon_r}+\tau)(1-\sqrt{\epsilon_r}+\tau)}. \end{aligned} \tag{5.33}$$

Similarly, the interference gain is given by

$$\begin{aligned} G_{int}^{WLRZF} &= \mathrm{E}\left\{ \frac{1}{P_r}\sqrt{\frac{P_{WLRZF}}{L}}\underline{g}_i\underline{h}_j \right\} \ \forall \ j\neq i = 1,\ 2, \ldots L \\ &= \frac{1}{P_r}\sqrt{\frac{P_{WLRZF}}{L}}(\Xi \ \mathrm{E}\{\underline{h}_i^H\underline{h}_j\} + \xi \ \mathrm{E}\{\sum_{l=1\neq i}^{}\sum_{k=1}^{N} h_{lk}^* h_{jk}\}) \\ &= \frac{1}{P_r}\sqrt{\frac{P_{WLRZF}}{L}}(\Xi\sqrt{\epsilon_q} + \xi(1+(L-2)\sqrt{\epsilon_q}) \\ &= \frac{1}{P_r}\sqrt{\frac{P_{WLRZF}}{L}}\frac{\tau((1+\tau)\sqrt{\epsilon_q}-\sqrt{\epsilon_r})}{(1+(L-1)\sqrt{\epsilon_r}+\tau)(1-\sqrt{\epsilon_r}+\tau)}. \end{aligned} \tag{5.34}$$

□

We also note that Theorems 1 and 2 can be used to convert between equivalent values of ϵ_r and ϵ_q for a given $Pr[\mathscr{S}_\epsilon \neq \{\emptyset\}]$, or $p_\perp$.

5.4.4 Numerical results

We investigate Proposition 1 numerically to gain further insights. Gain terms G_{sig}^{RZF} and G_{int}^{RZF} from Proposition 1 are plotted in left-hand and right-hand plots of Fig. 5.1, respectively, for various values of regularizing factor, τ.

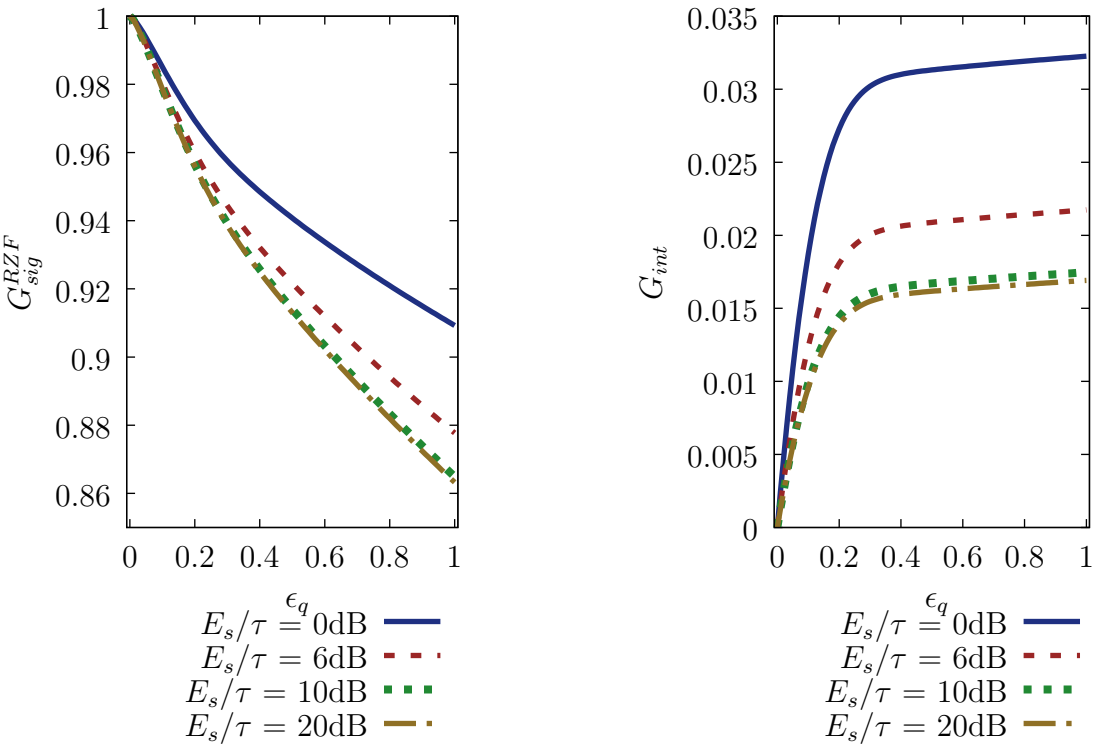

Figure 5.1: Analytic RZFBF of signal (left) and interference (right) gains from Proposition 1 as a function of ϵ_q, $L = 4$, $N = 16$, $P_{RZF} = L$..

The G_{sig}^{RZF} curves plotted in the left-hand plot of Fig. 5.1 decreases as ϵ_q increases. This trend agrees with expected behaviour: as interference in the system increases, the signal gain is sacrificed to mitigate interference. We observe that G_{sig}^{RZF} has a stronger dependency on ϵ_q for low τ than for high τ. This is characterized by a greater decrease in G_{sig}^{RZF} for low τ than for high τ, observed in the left-hand plot of Fig. 5.1. In one respect this agrees with expectations: we expect G_{sig}^{RZF} to converge to G_{sig}^{MRT} in high τ, thus explaining the behaviour we see in this curve. However, a lower G_{sig}^{RZF} for low τ than for high τ is somewhat counter-intuitive as it suggests lower system performance in low τ than for high τ. However, we are only considering part of the system, we should also consider the behaviour of G_{int}^{RZF} in the right-hand plot

of Fig. 5.1 to observe a more complete characterization of the system performance.

In contrast to the left-hand plot in Fig. 5.1, we observe that G_{int}^{RZF} increases with ϵ_q in the right-hand plot of Fig. 5.1. Since ϵ_q is a measure of interference in the system, this agrees with what we expect. We also observe that high τ curves experience larger interference than low τ curves. This agrees with intuition: high τ translates low SNR to relatively poor system performance. It is important to note that G_{int}^{RZF} values are scaled by a sum of $L-1$ interfering symbols, whereas G_{int} is only scaled by a single symbol. We expect the interference experienced by the system to be higher in this sense. Therefore, comparing the left-hand and right-hand plots of Fig. 5.1 directly is an unfair comparison of system performance. Thus, we expect the superior interference performance of low τ curves in the right-hand plot of Fig. 5.1 to compensate for the inferior signal performance of low τ curves in Fig. 5.1, resulting in superior system performance at high SNR than at low SNR.

Chapter 6

System Performance Analysis

System performance is analyzed in terms of reliability, efficiency and throughput using several metrics. Reliability and efficiency of transmission in the system are evaluated in terms of symbol error rate (SER) assuming no channel coding (as this analysis is at the physical layer). Single-user outage rate is selected as a metric to evaluate single-user throughput. Lastly throughput of the group is evaluated in terms of mean group sum rate. Performance analysis depends on many factors outlined in previous chapters including choice of modulation, beamforming, and ϵ-orthogonality; not to mention parameters such as number of antennas, group size, and number of candidates that impact these schemes, themselves. Thus, there are many valid permutations of these choices in the larger system. In order to manage these permutations, the system model of interest is classified as either a QVS or RVS model and performance is presented through the lens of this classification.

6.1 Symbol Error Rate

An analytic approach is taken in computing SER. We define $f_{R_i|S_i}(r_i \mid s_i)$ as the interference-averaged PDF of the i^{th} user's noisy received signal conditioned on the

transmission of a given symbol from Eq. (3.9). Assuming uniform transmission probability of symbols in the constellation, the SER is computed as

$$SER = \frac{1}{M}\sum_{l=1}^{M}\sum_{k=1\neq l}^{M}\int_{\mathcal{R}_k} f_{R_i|S_i}(r_i|\ s_i = \mathsf{s}_{(l)})\ dr_i \quad , \tag{6.1}$$

where $\mathcal{R}_1, \mathcal{R}_2, \ldots\ \mathcal{R}_M$ are the Voronoi regions of the constellation. A constant transmission power and noise power spectral density (i.e. constant SNR) is also assumed over the integration. Let us define the interference random variable Z_i with realizations $z_i \in Z_i$. Similarly, we define $f_{Z_i}(z_i)$ as the PDF of Z_i, and $f_{R_i|Z_i}(r_i|z_i)$ as R_i's PDF conditioned on Z_i. The PDF $f_{R_i|S_i}(r_i|s_i)$ can be computed as

$$f_{R_i|S_i}(r_i|s_i) = \sum_{z_i \in Z_i} f_{R_i|Z_i,S_i}(r_i|z_i, s_i) f_{Z_i}(z_i). \tag{6.2}$$

From Eq. (3.9) we let $Z_i = \sum_{j=1\neq i}^{L} \underline{w}_i \underline{h}_j S_j$, thus representing the interference for the i^{th} user in the group. Assuming a given transmit symbol for each of the users in the group and AWGN, we have $R_i \sim \mathcal{N}_{\mathbb{C}}(\underline{w}_i \underline{h}_i s_i + z_i, \mathbf{R})$ for quadrature modulated symbols and $R_i \sim \mathcal{N}(\underline{w}_i \underline{h}_i s_i + z_i, \sigma_n^2)$,where $\mathbf{R} = \frac{1}{2}\sigma_n^2 \mathbf{I}_2$ and $\mathbf{I}_2$ is the 2×2 identity matrix, $\mathcal{N}_{\mathbb{C}}(\mu, \nu\mathbf{I}_2)$ is a circular-symmetric complex normal distribution with mean μ and co-variance matrix $\nu\mathbf{I}_2$, and $\mathcal{N}(\mu, \nu)$ is a scalar normal distribution with mean μ and variance ν.

6.1.1 SER for maximum interference power case

SER can be computed as a function of G_{int} and G_{sig} assuming the maximum interference power scenario. Given an ϵ-orthogonal group in the context of QVS and RVS

models we have

$$Z_i = G_{int} \sum_{j \neq i}^{L} S_j \tag{6.3}$$

Symbols belonging to the j^{th} user in the ϵ-orthogonal group, given by $S_j,\ j \neq i$, can take one of M values from the constellation. It is assumed all users in the group use the same modulation scheme . We also assume $s_j \in S_j$ is realized from the set of possible symbols in the constellation with uniform probability. The sum in Eq. (6.2) is taken over $L-1$ users' interfering symbols. Therefore, the result of the sum may take M^{L-1} different values. Furthermore, the probability of each such result is uniform since the distribution of the arguments sum are uniform themselves. Therefore the PMF of Z_i follows the uniform distribution

$$f_{Z_i}(z_i) = \frac{1}{M^{L-1}} \int_{-\infty}^{\infty} \delta(x - z_i)dx \ \forall \ z_i \in Z_i, \tag{6.4}$$

where $x \in \mathbb{R}$ for amplitude modulation, and $x \in \mathbb{C}$ for quadrature modulation, and $\delta(\cdot)$ is the Dirac Delta funciton. Thus, $f_{R_i|S_i}(r_i \mid s_i)$ for QVS and is given by

$$\begin{aligned} f_{R_i|S_i}(r_i \mid s_i) = \frac{1}{M^{L-1}} \sum_{z_i \in Z_i} & \frac{1}{2\pi \det(\mathbf{R})} \\ & \exp\Big(- (r_i - G_{sig}s_i - z_i)^* \mathbf{R}^{-1} (r_i - G_{sig}s_i - z_i) \Big). \end{aligned} \tag{6.5}$$

Similarly, for RVS we have

$$f_{R_i|S_i}(r_i \mid s_i) = \frac{1}{M^{L-1}} \sum_{z_i \in Z_i} \frac{1}{\sqrt{2\pi\sigma_n^2}} \exp\Big(- \frac{(r_i - G_{sig}s_i - z_i)^2}{2\sigma_n^2} \Big). \tag{6.6}$$

6.1.2 Numerical results for maximum interference power case

Numerical SER performance is investigated as a function of interference in terms of ϵ_q for QVS models and ϵ_r for RVS models. We adopt a logarithmic SIR measure as a function of these parameters in order to generate conventional log-log plots of SER in Figs. 6.1-6.3.

We begin by considering the impact of the number of antennas on SER performance. SER is plotted as a function of SIR measure for various numbers of antennas and MRTBF assuming a RVS model in Fig. 6.1. The left-hand side of both plots in Fig. 6.1 is characterized by a lax constraint on orthogonality, associated with higher levels of interference in the system. Conversely, the right-hand side of both plots in Fig. 6.1 is characterized by a higher degree of orthogonality between users and low levels of interference in the system.

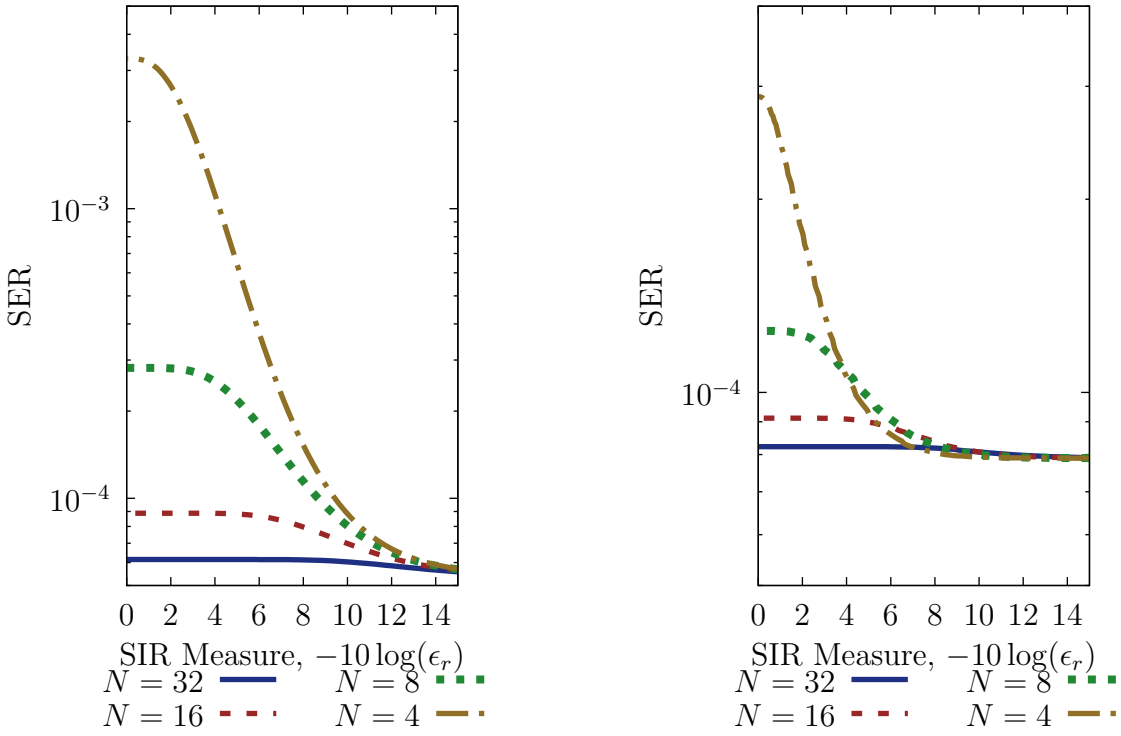

Figure 6.1: RVS SER given by Eq. 6.1 plotted against SIR measure in terms of ϵ_r for various numbers of antennas WL-MRTBF (left) and WL-RZFBF (right). BPSK, SNR = 10dB, $L = 8$, and $\tau = \sigma^2$ are assumed.

From both plots in Fig. 6.1, it is clear that SER performance improves as the constraint on orthogonality between users becomes more strict. This agrees with expected behaviour, since the amount of interference in the system decreases as orthogonality between users increases. Reduced interference translates to improved SER performance. Comparing the curves in either plot in Fig. 6.1, it is clear that the number of antennas in the system, N, has an impact on SER performance. More specifically, we notice that SER performance improves as N increases. Again, this agrees with expected behaviour, since the beamformer is able to take advantage of additional degrees of freedom provided by having more antennas than users in the

group to mitigate interference. We also observe that the $N = L = 4$ curves in Fig. 6.1 exhibit the strongest dependence on ϵ_r. In other words, when the degrees of freedom in the beamformer are small, user orthogonality assists the beamformer in mitigating interference. When many antennas are present and the group size is small, the beamformer is able to achieve adequate SER performance independent of user orthogonality. The $N = 16$ and $N = 32$ curves are associated with systems similar to a massive-MIMO scenario. In systems where the number of antennas, N, is much larger than the group size, L, the beamforming lobes become less isotropic and more focused. Therefore, interference between lobes transmitting to various users is reduced with the number of antennas, resulting in weaker dependence on user orthogonality.

We also note that the SER curves approach a SER floor for high SIR measure values. This behaviour is explained by the fact that SER curves are plotted with a constant SNR. When the SIR measure becomes large, the SER performance is limited by noise rather than interference. Therefore, for high SIR values, the SER performance approaches a floor resulting from the assumption of constant SNR.

Next we compare QVS and RVS SER results. The number of users in the ϵ-orthogonal group, L, depends on the modulation scheme in order to ensure constant maximum achievable group sum rate in the group. A maximum group sum rate of 8 bits/channel use is assumed for each curve in order to make a fair comparison.

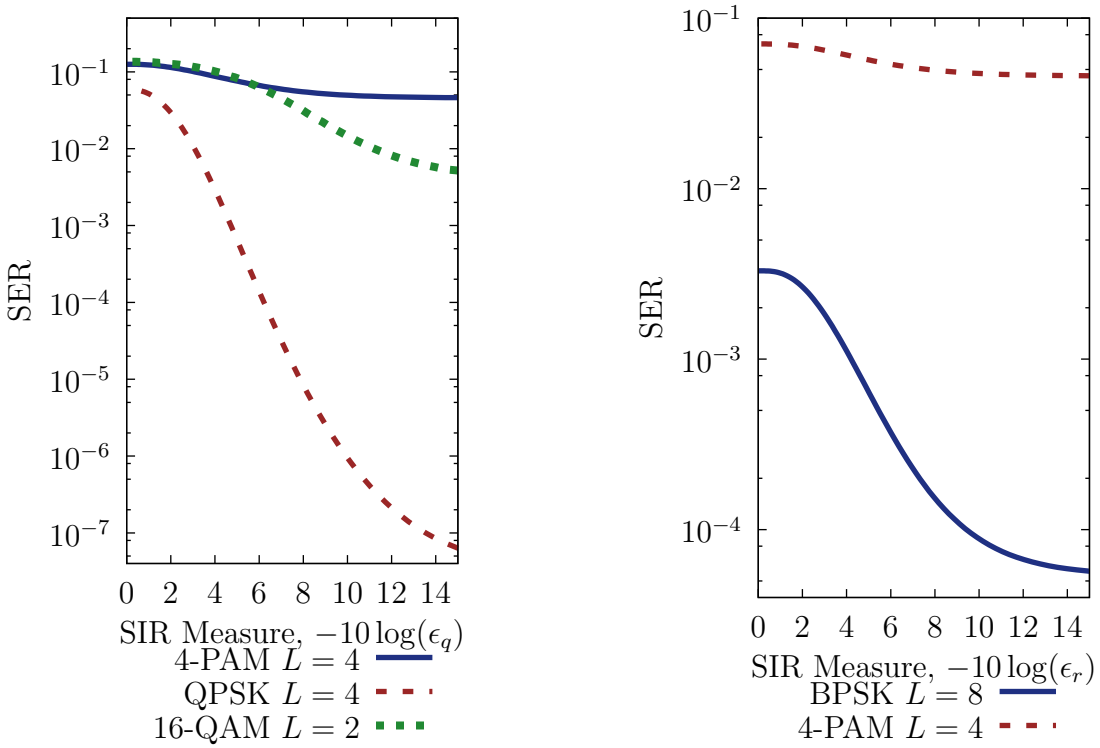

Figure 6.2: QVS SER given by Eq. 6.1 (left plot) plotted against SIR measure in terms of ϵ_q. MRTBF, SNR = 10dB, and $N = 4$ are assumed. RVS SER given by Eq. 6.1 (right plot) plotted against SIR measure in terms of ϵ_r. WL-MRTBF, SNR = 10dB, and $N = 4$ are assumed.

From Fig. 6.2, we observe that QPSK is able to achieve better SER performance than 4-PAM and 16-QAM. The SER curves are plotted for constant symbol energy. This illustrates the expected power efficiency-spectral efficiency trade-off. We notice the presence of a curve corresponding to BPSK modulation in the RVS plot of Fig. 6.2. No BPSK curve was included in the QVS plot of Fig. 6.2 because MRTBF can only support $L = 4$ users for $N = 4$. Thus, the maximal sum rate for such a group assuming BPSK is 4 bits/channel use. Making comparisons to other curves in this context is unfair since these schemes all correspond to a maximum sum rate of 8

bits/channel use. However; in WL-MRTBF assumed in the RVS model corresponding to Fig. 6.2, the beamforming scheme can support $L = 2N = 8$. Therefore, inclusion of such a curve is fair in the maximum sum rate sense. We also notice a small improvement in SER performance in the 4-PAM RVS curve compared to the 4-PAM QVS curve in high interference.

Plots of QVS and RVS SER performance for RZFBF are shown in Fig. 6.3. The same schemes and parameters are assumed as in Fig. 6.2 with the exception of beamforming.

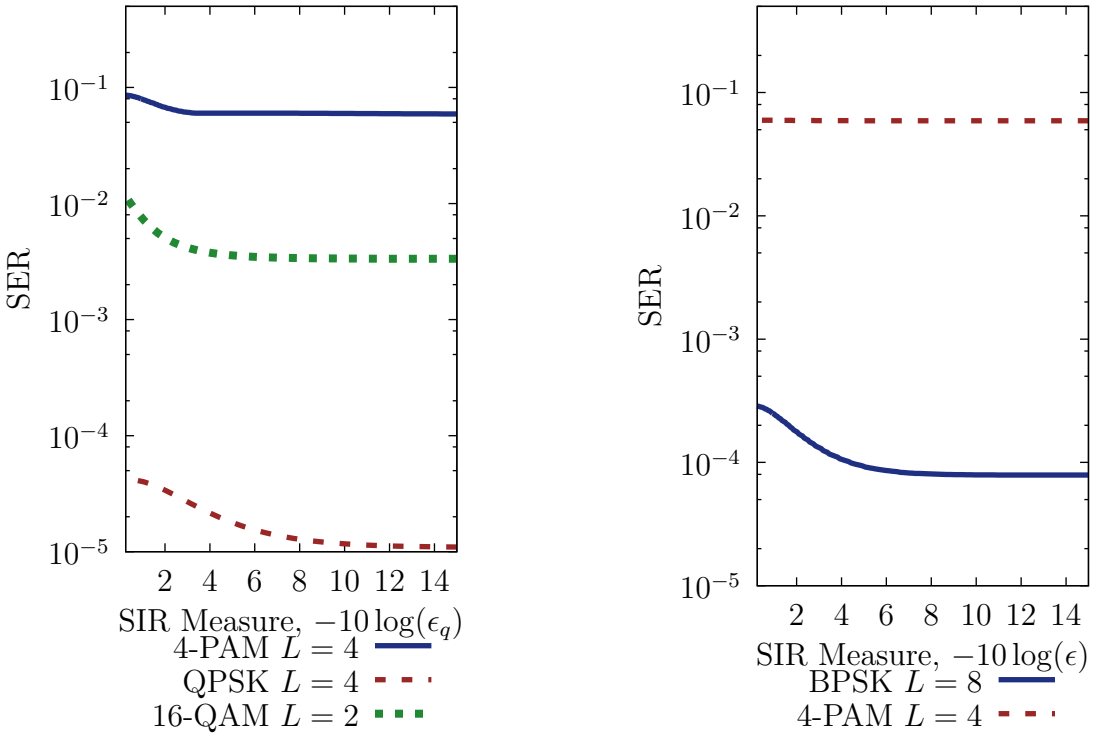

Figure 6.3: QVS SER given by Eq. 6.1 (left) plotted against SIR measure in terms of ϵ_q. RZFBF, SNR = 10dB, and $N = 4$ are assumed. RVS SER given by Eq. 6.1 (right) plotted against SIR measure in terms of ϵ_r. WL-RZFBF, SNR = 10dB, $N = 4$, and $\tau = \sigma^2$ are assumed.

Comparing the QVS and RVS plots in Fig. 6.3, we observe consistent behaviour with previous QVS-RVS comparisons in Figs. 6.2. The RZFBF curves in Fig. 6.3 are less dependent on user selection than MRTBF curves in Fig. 6.2. This agrees with expected behaviour since the RZFBF scheme mitigates interference while the MRTBF neglects interference. Thus, constraining user orthogonality has a greater impact on MRTBF SER performance than RZFBF SER performance.

6.2 Outage rate

Single-user throughput is evaluated in terms of outage rate. We begin by defining a Bernoulli-distributed outage event, O; $O = 1$ when the system is in an outage and $O = 0$ when the system is not in an outage. When the system is in an outage, we assume the system is unable to transmit data. Conversely, when the system is not in an outage, the system is able to transmit $\log_2(M)$ bits/channel use to a given user in the group. We define SER_o as the outage SER of the system. SER_o is the reliability metric required to transmit without outage. There is a reliability-throughput trade-off in the model. The system is able to achieve a high degree of reliability (i.e. low SER_o value) for low throughput (i.e. outage rate) values without being in outage. Conversely, a high outage rate is achievable with a low SER_o value without the system being in an outage.

SER_o can then be mapped back to an outage interference we define as v_o. We adopt a notation similar to Eq. (4.3, that is $v_o \in \{v_{o_q},\ v_{o_r}\}$), where v_{o_q} is the QVS outage interference and v_{o_r} is the RVS outage interference. The probability of an outage is computed by integrating the domain of the PDF belonging to interference values that exceed the permissible outage interference. Following this approach, the

probability of an outage event is given as

$$Pr[O = 1] = \int_{v_o}^{1} f_V(v)\ dv \quad . \tag{6.7}$$

Given a modulation scheme with M symbols, We can write the single-user outage rate for a given user as

$$\begin{aligned} C_o &= \log_2(M)(1 - Pr[O = 1]) + 0 \cdot (Pr[O = 1]) \\ &= \log_2(M)(1 - Pr[O = 1]), \end{aligned} \tag{6.8}$$

C_o is also Bernoulli-distributed, as implied by Eq. (6.8). It is also implied that the equality in Eq. (6.8) is conditioned on the existence of an ϵ-orthogonal group.

6.2.1 Numerical results for maximum interference power case

Single-user outage rate is plotted as function of interference, in terms of ϵ, in Fig. 6.4. C_o is plotted for for various modulation schemes belonging to RVS and QVS models. RZFBF is assumed for QVS curves, while WL-RZFBF is assumed for RVS curves. The left-hand side of the plot is characterized by low interference in the system, while the right-hand side of the plot is characterized by high interference in the system.

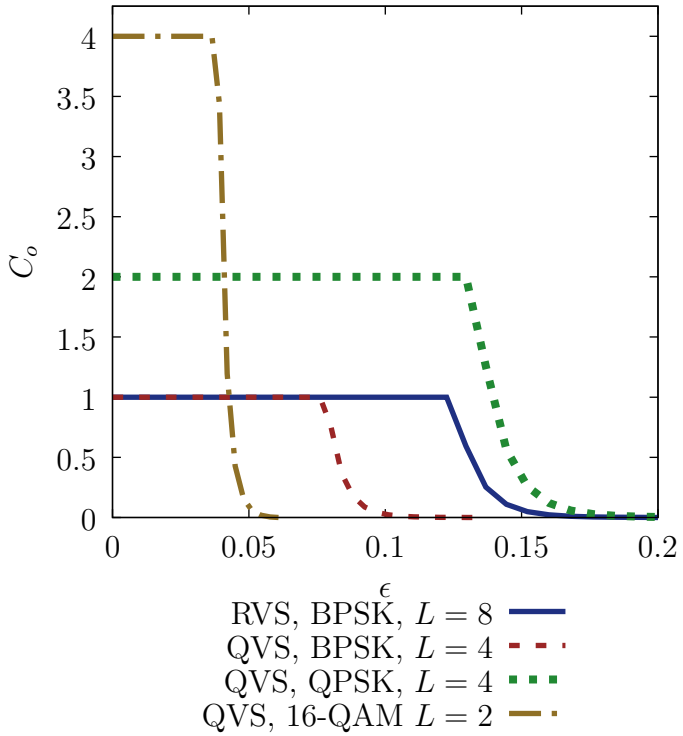

Figure 6.4: RVS and QVS single-user outage rate (bits per channel use) given by Eq. (6.8) plotted as a function of user orthogonality constraint ϵ. RZFBF assumed for QVS, WL-RZFBF assumed for RVS, $N = 16$, SNR= 10dB, and $\tau = \sigma^2$.

Several observations can be made from the curves plotted in Fig. 6.4. Firstly, we notice that rate is a monotonically decreasing function of interference; as interference increases, rate decreases. We also notice that all modulation schemes are able to achieve theoretical maximum rate if the constraint on user orthogonality is as strict as possible (i.e. $\epsilon = 0$) and interference in the system is eliminated. Comparing the RVS and QVS BPSK curves is not fair in terms of achievable sum rate: the RVS curve has twice as many users in the group compared to the QVS curve. However, this comparison favours the QVS curve, since the RVS curve will experience more interference from the additional users in the group; yet, the RVS curve is still more resilient to

interference than the QVS curve. This performance difference is illustrated by the BPSK RVS curve achieving superior C_o than the QVS BPSK curve for larger values of ϵ. Since the REO group criterion in Definition 3 only cares about the real part of the inner product rather than the magnitude, it is able to sustain larger amounts of interference relative to the QEO definition while achieving the same throughput performance.

6.3 Mean Sum Rate

The sum rate of the ϵ-orthogonal group is calculated as the sum of the single-user outage rates belonging to users in the group. The outage rate for each user in the group is assumed to be statistically independent assuming spatial separation of users. Thus, the sum rate is a sum of L independent Bernoulli random variables, and therefore, follows a binomial distribution whose mean can be calculated using Eqs. (4.54) and (6.8) and is given by

$$\begin{aligned} \mathrm{E}\{SR\} &= L \cdot C_o \cdot Pr[\mathscr{S}_\epsilon \neq \emptyset] \\ &= L \cdot \log_2(M)(1 - Pr[O]) \cdot Pr[\mathscr{S}_\epsilon \neq \emptyset]. \end{aligned} \tag{6.9}$$

6.3.1 Numerical results for maximum interference power case

Numerical mean sum rates for ϵ-orthogonal groups are computed using Eq. 6.9 and presented for QVS, then RVS models in the following figures. The numerical results assume a dense deployment of users with many candidate users available; therefore, $K = 30$ candidate users are assumed. A MIMO transmitter with $N = 16$ antennas is assumed. In order to make fair comparisons, we assume that the same theoretical maximum sum rate is achievable for each group. Thus, the number of users in the

group depends on the modulation scheme. A theoretical maximum sum rate of 8 bits/channel use is assumed. We begin by investigating the QVS model assuming MRTBF in Fig. 6.5.

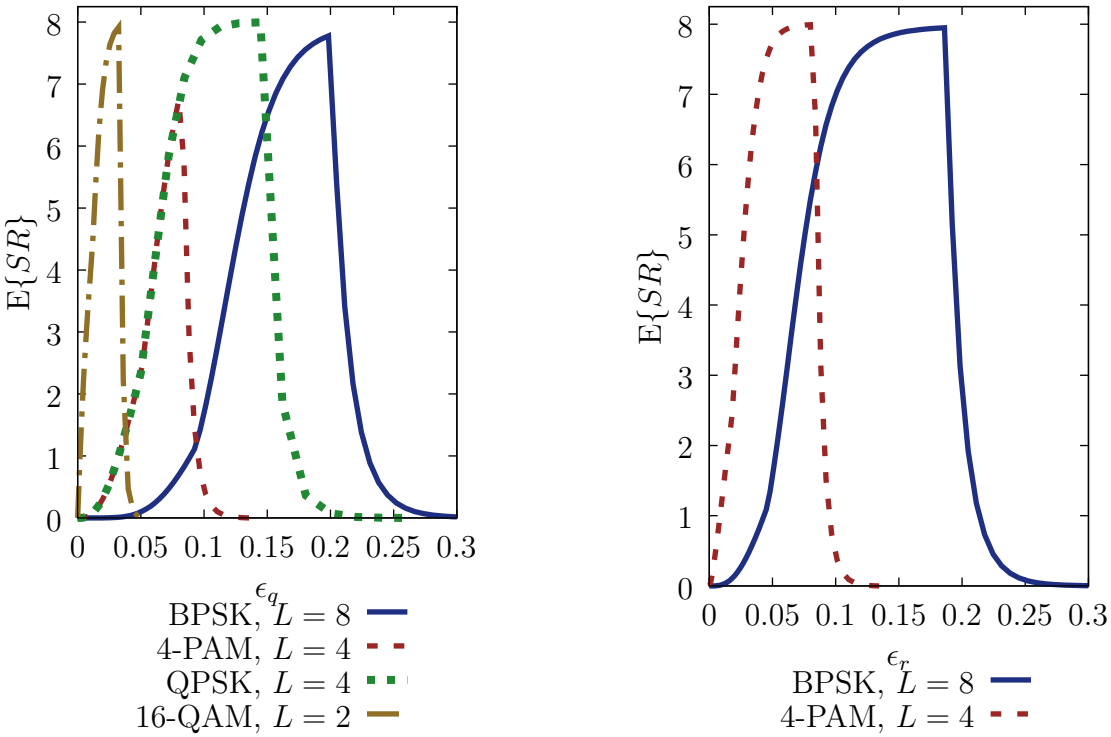

Figure 6.5: QVS mean sum rate (bits per channel use) given by Eq. (6.9) (right plot) plotted as a function of ϵ_q for MRTBF. $N = 16$, $K = 30$, SNR=10dB. RVS mean sum rate (bits per channel use) given by Eq. (6.9) (left plot) plotted as a function of ϵ_r for WL-MRTBF. $N = 16$, $K = 30$, SNR=10dB.

From Fig. 6.5, we notice that peak sum rate is achieved in both RVS and QVS models at an intermediate value of ϵ. That is, the constraint on user orthogonality should be neither too strict, nor too lax. The domain of the user orthogonality parameter is $\epsilon \in [0, 1]$. From Fig. 6.5, we notice that peak mean group sum rates are achieved towards lower end of this domain, indicating there are performance benefits

associated with being selective with the users we admit to the group. These performance benefits are only enjoyed up to a point. If the user orthogonality constraint is too demanding, it is unable to find users to add to the group, and system throughput performance suffers.

We also notice from Fig. 6.5 that the peak sum rate depends on the modulation scheme. There are several reasons for this behaviour. The number of users in the group depends on the modulation scheme in order to make fair sum rate comparisons. High-order modulation schemes have fewer users in a group. Since there are fewer users in the group, it is much easier to find an ϵ-orthogonal group as computed in Chapter 4; intuitively, fewer users need to be mutually ϵ-orthogonal for a small group, thus, we have a higher probability of finding a group with fewer users in it. This behaviour is clearly illustrated in Fig. 6.5. Consider the 16-QAM and BPSK curves in the QVS plot of Fig. 6.5. We observe that peak sum rate is achieved at $\epsilon_q = 0.03$ for 16-QAM compared to $\epsilon_q = 0.19$ for BPSK. Therefore, as Fig. 6.5 illustrates, these schemes are able to achieve mean sum rates near the theoretical maximum for a given reliability metric; however, the value of ϵ_q that corresponds to these peak mean sum rates depends on the modulation scheme.

Comparing mean sum rates in the RVS plot of Fig. 6.5 for BPSK and 4-PAM to QVS BPSK and 4-PAM sum rates in Fig. 6.5 there are advantages associated with RVS BPSK and 4-PAM compared to QVS BPSK and 4-PAM. A siginificant advantage of RVS over QVS demonstrated by Fig. 6.5 is system tunability. Wider sum rate peaks in Fig. 6.5 represent better system tunability: high mean sum rate is achievable over a wider range of ϵ. We define the system tunability as the range of ϵ that allows the system to achieve $\mathrm{E}\{SR\} \geq 4$ bits/channel use (50% of theoretical

maximum in the scenarios investigated). Comparing the QVS and RVS mean sum rates for BPSK and 4-PAM in Fig. 6.5, the QVS models have a system tunability of 0.08 and 0.04 for BPSK and 4-PAM respectively; whereas RVS models have a system tunability of 0.13 and 0.07 for BPSK and 4-PAM respectively. We also note that 4-PAM QVS is only able to achieve a peak mean sum rate of 6.51 bits/channel use, compared to 7.97 bits/channel use for RVS 4-PAM.

We perform a similar investigation assuming RZFBF in Fig. 6.6. All parameters are held the same in Fig. 6.6 as Fig. 6.5 with the exception of the beamforming scheme assumed.

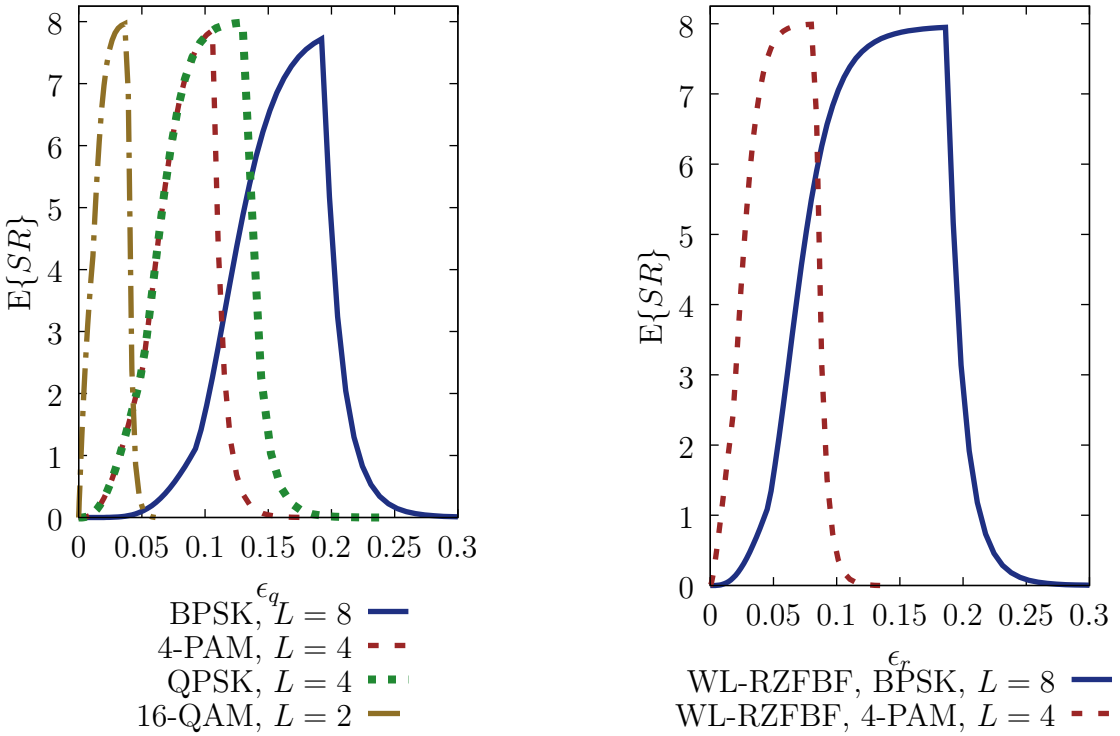

Figure 6.6: QVS mean sum rate (bits per channel use) given by Eq. (6.9) (left plot) plotted as a function of ϵ_q for RZFBF, $N = 16$, $K = 30$, SNR=10dB. RVS mean sum rate (bits per channel use) given by Eq. (6.9) (right plot) plotted as a function of ϵ_q for WL-RZFBF, $N = 16$, $K = 30$, SNR=10dB, and $\tau = \sigma^2$

Again, we observe superior system tunability for RVS compared to QVS. QVS achieves a system tunability of 0.09 and 0.07 for BPSK and 4-PAM, respectively, compared to RVS system tunability of 0.13 and 0.08 for BPSK and 4-PAM, respectively.

Chapter 7

Conclusions and Future Work

7.1 Conclusions

The key aspect of this work is the analyses of ϵ-orthogonal group existence for REO and QEO groups. The investigation includes both analytic and numerical approaches to this problem. This analysis is not limited to a specific user selection algorithm, rather is provides insights into the concepts underpinning many practical user selection algorithms designed to mitigate interference. In order to put this analysis in context, a throughput analysis is required. We develop an average-basis throughput analysis where all the interference powers amongst the group of users are equal, where the interference power is the maximum tolerable interference for a given user orthogonality constraint in the group. This special case is of particular interest for a system implementing a user selection scheme. Many aspects of the throughput analysis are not limited by the special uniform interference case investigated in this work and could be extended.

The throughput analysis presented in this work illustrates how a judicious choice of modulation, user orthogonality criteria, and beamforming can be made to meet a

wide range of QoS requirements in future wireless networks. Results illustrate that by relaxing user orthogonality criteria for amplitude-modulated systems, a higher probability of finding a large group of users is achieved. Moreover, using widely-linear beamforming schemes, such a group can achieve concurrent service from a transmitter with a relatively low number of antennas. Conversely, results illustrate quadrature-modulated systems, which require more strict user orthogonality criteria relative to amplitude-modulated systems, have a lower probability of finding a group of the same size. However, fewer users are needed to achieve comparable spectral efficiency in the high-order quadrature modulated system compared to the low-order amplitude modulated system, thus increasing the probability of finding a group. This behaviour characterizes an application-specific trade-off: systems using high-order quadrature modulation are well-suited to high-throughput, high-latency QoS applications, while systems using low-order amplitude modulation are better suited to low-throughput, low-latency applications.

7.2 Future Work

Further work to generalize and extend the existing work is recommended. Several useful generalizations of the model include modelling non-uniform interference in the group, line-of sight propagation, and non-isotropic antennas. The joint beamforming user orthogonality analysis in this work assumes uniform interference amongst users in the group. Although this is an interesting and useful scenario for system performance analysis, a non-uniform interference model is more realistic, although less simplistic. Modelling line-of-sight propagation is also a useful extension of the work. Incorporating line-of-site propagation into the analysis would not only make

the model more flexible, it would also allow for better modelling of massive MIMO systems. Further work is also recommended in addressing challenges specific to massive MIMO applications as discussed in [45]. Furthermore, the existing work could also be generalized further by considering non-isotropic antennas.

In addition to the recommended generalizations and extensions, the existing work could also be applied to the development of new work including improved user selection algorithms, and inter-cellular interference mitigation algorithms in the wireless downlink physical layer. A significant portion of the existing work is dedicated to modelling the interference between users statistically. The statistical analysis could be used to develop improved user selection algorithms. For example, one could view the user selection algorithm as an optimal stopping problem: after considering a number of candidates for the group, the complexity of continuing the search out-weighs the benefits of continuing. The statistical analysis developed in this work could be used to quantify this trade-off for both quadrature and amplitude-modulated users. The existing work focuses on intra-cellular interference mitigation. However, the work could be applied to inter-cellular interference mitigation in the wireless downlink as well. For example, in a centralized network with coordination between overlapping cells, ϵ-orthogonal user criteria could be used to reduce complexity in inter-cellular interference mitigation algorithms. Similarly, the existing work could be used to develop an distributed interference mitigation algorithm when there is no coordination between cells. For example, cost and reward functions could be described in terms of ϵ-orthogonality in a distributed reinforcement learning algorithm.

Bibliography

[1] F. Jejdling, P. Cerwall, A. Lundvall, S. Carson, P. Jonsson, R. Moller, A. Torres, P. Lindberg, K. Ohman, A. Karapantelakis, S. Bajgin, E. Purtova, S. Sezgin Alp, M. Karakoc, G. Yardim, and J. Barbour, "Ericsson Mobility Report June 2019," Telefonaktiebolaget LM Ericsson, Tech. Rep., 2019.

[2] Cisco Networks, "Cisco visual networking index: Global mobile data traffic forecast update, 2017-2022," Cisco Networks, Tech. Rep., 2019.

[3] 5G-PPP Architecture Working Group, "View on 5G architecture," 5G-PPP, Tech. Rep., 2018.

[4] A. Yastrebova, R. Kirichek, Y. Koucheryavy, A. Borodin, and A. Koucheryavy, "Future networks 2030: Architecture requirements," in *2018 10th International Congress on Ultra Modern Telecommunications and Control Systems and Workshops (ICUMT)*, Nov 2018, pp. 1–8.

[5] N. ul Hasan, W. Ejaz, I. Baig, M. Zghaibeh, and A. Anpalagan, "QoS-aware channel assignment for IoT-enabled smart building in 5G systems," in *2016 Eighth International Conference on Ubiquitous and Future Networks (ICUFN)*, July 2016, pp. 924–928.

[6] A. Emarievbe, J. Koepp, and T. Opferman, "Emerging communication technologies enabling the internet of things," Rhode and Schwarz, Tech. Rep., 2016.

[7] S. Sun, T. S. Rappaport, R. W. Heath, A. Nix, and S. Rangan, "MIMO for millimeter-wave wireless communications: beamforming, spatial multiplexing, or both?" *IEEE Communications Magazine*, vol. 52, no. 12, pp. 110–121, December 2014.

[8] M. Xiao, S. Mumtaz, Y. Huang, L. Dai, Y. Li, M. Matthaiou, G. K. Karagiannidis, E. Bjrnson, K. Yang, C. I, and A. Ghosh, "Millimeter wave communications for future mobile networks," *IEEE Journal on Selected Areas in Communications*, vol. 35, no. 9, pp. 1909–1935, Sep. 2017.

[9] S. Nam, J. Kim, and Y. Han, "A user selection algorithm using angle between subspaces for downlink mu-mimo systems," *IEEE Transactions on Communications*, vol. 62, no. 2, pp. 616–624, February 2014.

[10] G. Gupta and A. K. Chaturvedi, "User selection in MIMO interfering broadcast channels," *IEEE Transactions on Communications*, vol. 62, no. 5, pp. 1568–1576, May 2014.

[11] Z.Shen, R. Chen, J. G. Andrews, R. W. Heath, and B. L. Evans, "Low complexity user selection algorithms for multiuser mimo systems with block diagonalization," *IEEE Transactions on Signal Processing*, vol. 54, no. 9, pp. 3658–3663, Sep. 2006.

[12] C. Swannack, E. Uysal-Biyikoglu, and G. W. Wornell, "Finding NEMO: near mutually orthogonal sets and applications to MIMO broadcast scheduling," in

2005 International Conference on Wireless Networks, Communications and Mobile Computing, vol. 2, June 2005, pp. 1035–1040 vol.2.

[13] S. Li, "Concise formulas for the area and volume of a hyperspherical cap," *Asian Journal of Mathematics & Statistics*, vol. 4, 01 2011.

[14] R. J. Muirhead, *Aspects of multivariate statistical theory*, ser. Wiley series in probability and mathematical statistics. Probability and mathematical statistics. Wiley, 1982.

[15] A. K. Gupta and S. Nadarajah, *Handbook of Beta Distribution and its Applications*. New York, NY, USA: Marcel Dekker, Inc., 2004.

[16] T. Adali, P. J. Schreier, and L. L. Scharf, "Complex-valued signal processing: The proper way to deal with impropriety," *IEEE Transactions on Signal Processing*, vol. 59, no. 11, pp. 5101–5125, Nov 2011.

[17] B. Picinbono and P. Chevalier, "Widely linear estimation with complex data," *IEEE Transactions on Signal Processing*, vol. 43, no. 8, pp. 2030–2033, Aug 1995.

[18] P. Chevalier and F. Pipon, "New insights into optimal widely linear array receivers for the demodulation of bpsk, msk, and gmsk signals corrupted by noncircular interferences-application to saic," *IEEE Transactions on Signal Processing*, vol. 54, no. 3, pp. 870–883, March 2006.

[19] C. E. Shannon, "Probability of error for optimal codes in a Gaussian channel," *The Bell System Technical Journal*, vol. 38, no. 3, pp. 611–656, May 1959.

[20] A. Fazeli, A. Vardy, and E. Yaakobi, "Generalized sphere packing bound," *IEEE Transactions on Information Theory*, vol. 61, no. 5, pp. 2313–2334, May 2015.

[21] P. J. Schreier and L. L. Scharf, *Statistical Signal Processing of Complex-Valued Data: The Theory of Improper and Noncircular Signals.* Cambridge University Press, 2010.

[22] W. Gardner, "Spectral correlation of modulated signals: Part i - analog modulation," *IEEE Transactions on Communications*, vol. 35, no. 6, pp. 584–594, June 1987.

[23] W. Gardner, W. Brown, and Chih-Kang Chen, "Spectral correlation of modulated signals: Part ii - digital modulation," *IEEE Transactions on Communications*, vol. 35, no. 6, pp. 595–601, June 1987.

[24] J. G. Proakis and D. K. Manolakis, *Digital Signal Processing (4th Edition).* Upper Saddle River, NJ, USA: Prentice-Hall, Inc., 2006.

[25] E. Bjornson, M. Bengtsson, and B. Ottersten, "Optimal multiuser transmit beamforming: A difficult problem with a simple solution structure [lecture notes]," *IEEE Signal Processing Magazine*, vol. 31, no. 4, pp. 142–148, July 2014.

[26] S. Boumard, "Novel noise variance and SNR estimation algorithm for wireless MIMO OFDM systems," in *GLOBECOM '03. IEEE Global Telecommunications Conference (IEEE Cat. No.03CH37489)*, vol. 3, Dec 2003, pp. 1330–1334 vol.3.

[27] P. Chevalier, J. Delmas, and A. Oukaci, "Optimal widely linear MVDR beamforming for noncircular signals," in *2009 IEEE International Conference on Acoustics, Speech and Signal Processing*, April 2009, pp. 3573–3576.

[28] M. Bavand and S. D. Blostein, "User selection and widely linear multiuser precoding for one-dimensional signalling," *IEEE Transactions on Vehicular Technology*, vol. 67, no. 12, pp. 11 642 – 11 653, 2018.

[29] M. Bavand and S. D. Blostein, "Widely linear multiuser precoding for one-dimensional signalling," in *2018 52nd Asilomar Conference on Signals, Systems, and Computers*, Oct 2018, pp. 157–161.

[30] C. Hellings, M. Joham, and W. Utschick, "QoS feasibility in MIMO broadcast channels with widely linear transceivers," *IEEE Signal Processing Letters*, vol. 20, no. 11, pp. 1134–1137, Nov 2013.

[31] A. Medra and T. N. Davidson, "Widely linear interference alignment precoding," in *2014 IEEE 15th International Workshop on Signal Processing Advances in Wireless Communications (SPAWC)*, June 2014, pp. 464–468.

[32] T. Yoo, N. Jindal, and A. Goldsmith, "Multi-antenna downlink channels with limited feedback and user selection," *IEEE Journal on Selected Areas in Communications*, vol. 25, no. 7, pp. 1478–1491, September 2007.

[33] M. Min, Y. Jeon, and G. Im, "On achievable rate of user selection for MIMO broadcast channels with limited feedback," *IEEE Transactions on Communications*, vol. 65, no. 1, pp. 122–135, Jan 2017.

[34] Y. Liu, Z. Qin, M. Elkashlan, Z. Ding, A. Nallanathan, and L. Hanzo, "Nonorthogonal multiple access for 5G and beyond," *Proceedings of the IEEE*, vol. 105, no. 12, pp. 2347–2381, Dec 2017.

[35] R. Rajashekar and L. Hanzo, "User selection algorithms for block diagonalization aided multiuser downlink mm-Wave communication," *IEEE Access*, vol. 5, pp. 5760–5772, 2017.

[36] D. Ruyet, H. Khanfir, and B. Ozbek, "Performance of semi-orthogonal user selection for multiuser MISO systems," in *2008 International ITG Workshop on Smart Antennas*, 08 2008, pp. 321 – 325.

[37] W. Ni, Z. Chen, H. Suzuki, and I. Collings, "On the performance of semi-orthogonal user selection with limited feedback," *IEEE Communications Letters*, vol. 15, no. 12, pp. 1359–1361, 12 2011.

[38] S. M. R. Islam, N. Avazov, O. A. Dobre, and K. Kwak, "Power-Domain Non-Orthogonal Multiple Access (NOMA) in 5G Systems: Potentials and Challenges," *IEEE Communications Surveys Tutorials*, vol. 19, no. 2, pp. 721–742, Secondquarter 2017.

[39] A. D. Wyner, "Random packings and coverings of the unit n-sphere," *The Bell System Technical Journal*, vol. 46, no. 9, pp. 2111–2118, Nov 1967.

[40] S. Janson, "Large deviations for sums of partly dependent random variables," *Random Structures Algorithms*, vol. 24, pp. 234–248, 2004.

[41] M. E. Muller, "A note on a method for generating points uniformly on n-dimensional spheres," *Commun. ACM*, vol. 2, no. 4, pp. 19–20, Apr. 1959.

[42] C. B. Peel, B. M. Hochwald, and A. L. Swindlehurst, "A vector-perturbation technique for near-capacity multiantenna multiuser communication-part i: channel inversion and regularization," *IEEE Transactions on Communications*, vol. 53, no. 1, pp. 195–202, Jan 2005.

[43] B. M. Hochwald, C. B. Peel, and A. L. Swindlehurst, "A vector-perturbation technique for near-capacity multiantenna multiuser communication-part ii: perturbation," *IEEE Transactions on Communications*, vol. 53, no. 3, pp. 537–544, March 2005.

[44] E. Bjornson and E. Jorswieck, *Optimal Resource Allocation in Coordinated Multi-Cell Systems*, 01 2013, vol. 9.

[45] R. W. Heath Jr. and A. Lozano, *Foundations of MIMO Communication.* Cambridge University Press, 2018.